PAUL GIERZ

OCEAN CIRCULATION STABILITY UNDER POSSIBLE FUTURE CLIMATE SCENARIOS: LESSONS FROM A COUPLED ATMOSPHERE OCEAN CRYOSPHERE MODEL

OCEAN CIRCULATION STABILITY UNDER POSSIBLE FUTURE CLIMATE SCENARIOS: LESSONS FROM A COUPLED ATMOSPHERE OCEAN CRYOSPHERE MODEL

PAUL GIERZ
4287735

PROF. DR. BODO AHRENS

PROF. DR. GERRIT LOHMANN

A thesis submitted in fulfillment of the requirements for

Master of Science (M.Sc.)
Umweltwissenschaften
Universität Frankfurt

– Juni 2013 –

Paul Gierz: *Ocean Circulation Stability under Possible Future Climate Scenarios: Lessons from a Coupled Atmosphere Ocean Cryosphere Model*

ABSTRACT

Utilizing a novel setup of the COSMOS climate model including dynamic ice sheets, it is possible to directly evaluate the effect of future climate warming on the North Atlantic region. The dynamic ice sheets allow for the accurate simulation of meltwater injection from the Greenland Ice Sheet, effecting the salinity budget of critical deep water formation sites in the Nordic Seas. Given a strong enough perturbation of the salinity budget, the corresponding density of the upper ocean layers changes, resulting in a marked decrease in the Atlantic Meridional Overturning Circulation. This in turn has influences on the ability to transport heat from the equator towards the polar latitudes, resulting in far-reaching changes to the global climate system.

ZUSAMMENFASSUNG

Durch Nutzung des COSMOS Klimamodels, welches über eine dynamische Eisschildkomponente verfügt, ist es möglich direkte Effekte von Klimaerwärmung auf den Nordatlantik zu erkennen. Das dynamische Eisschild ermöglicht eine akurate Simulation von Süßwasserinjektionen in den Ozean, die durch Schmelzen des Grönlandeisschildes verursacht werden. Diese beeinflussen nicht nur den Salzhaushalt in den Nordischen Meeren, sondern auch die Dichte der oberen Ozeanschichten. Die für die Tiefenozeanzirkulation kritischen Tiefwasserbildungszonen werden dadurch gestört, und das gesamte Zirkulationssystem wird abgebremst. Dadurch wird die Fähigkeit des Ozeans, Wärme von dem Äquator zu den polaren Breiten zu transportieren nachteilig beeinflusst, welches weitreichende Folgen auf das gesamte Klimasystem hat.

The climate-studies people who work with models always tend to overestimate their models. They come to believe models are real and forget they are only models.

— Freeman Dyson

All models are wrong, but some are useful.

— George E. P. Box

ACKNOWLEDGMENTS

First and foremost I would like to thank my advisors, Prof. Gerrit Lohmann and Prof. Bodo Ahrens for giving me the opportunity to work on this project.

Additionally I would like to thank Dr. Martin Werner and Christian Stepanek for their insight and introducing me to the COSMOS climate model, Dr. Klaus Grosfeld, Dr. Malte Thoma and Dr. Dirk Barbi for helping me come to terms with the RIMBAY ice sheet model. Gregor Knorr and Conor Purcell afforded me many useful discussions regarding the mechanistic understanding required to comprehend freshwater injections and their effect on climate.

I'd also like to thank my friends and colleagues from the Paleoclimate Dynamics group for making my transition to the AWI easy and enjoyable. Finally I'd like to thank my friends and family for their continued support throughout my education.

CONTENTS

LIST OF FIGURES

LIST OF TABLES

ACRONYMS

AABW	Antarctic Bottom Water
AMOC	Atlantic Meridional Overturning Circulation
CMIP5	Coupled Model Intercomparison Project 5
ESM	Earth System Model
GHG	Greenhouse Gas
GIN	Greenland, Iceland, and Norwegian Seas
GIS	Greenland Ice Sheet
ISM	Ice Sheet Model
LAB	Labrador Sea
NADW	North Atlantic Deep Water
RCP	Representative Concentration Pathway
SIA	Shallow Ice Approximation
SSA	Shallow Shelf Approximation
THC	Thermohaline Circulation

1 INTRODUCTION

1.1 GENERAL BACKGROUND ON THE CLIMATE SYSTEM

Understanding the long-term consequences of climate change, both natural and anthropogenic, should be an important goal when faced with any question regarding climate change and variability. The ability to understand what causes certain stable outcomes within the climate system is crucial not only to the efforts of climate change mitigation or reduction, but should also play a role when policymakers make decisions regarding possible adaptations to inevitable climate changes. Understanding where, how, and to what extent the climate will alter its behavior based upon different forcings is one of the key goals of climate science research, and this thesis will examine one specific possible change in detail - the stability and potential change of ocean circulation in a warming future climate, as well as the consequences of this change.

Before beginning, the general components of the climate system are described as well as what their current mean states are. Next, the possibility of change within these components is discussed, and what this change might imply for the rest of the climate system.

1.1.1 Atmosphere

Perhaps the most immediately identifiable subsystem of the Earth's climate is the atmosphere. On short time scales changes in air pressure, temperature, and water content generate the weather we experience day to day. It should go without saying that daily weather plays an import role in our lives. Longer time scales allow for slow changes in what may be considered a "normal" weather cycle for a certain region. The average maximal temperature in summer or minimal temperature in winter can slowly change over time, as can the amount of rainfall that is to be expected in a given season.

If we examine the atmosphere based upon physical properties, a few things become apparent: in comparison to other climate components, the atmosphere is highly mobile, and mixes much faster than other components. A relatively small heat capacity allows for rapid temperature changes, and the chemical properties of several minor and trace components allow for residual greenhouse warming. The presence of aerosols facilitates the formation of clouds, temporarily changing the local albedo.

1.1.2 Ocean

The ocean is equally relevant, providing the largest reservoir of water on the planet. Having a high heat capacity, ocean circulation is responsible for heat transport between the poles and the equator, influencing the amount of thermal energy available at these locations. This can have profound implications; as an example, the heat transported from the equator towards the north pole in the North Atlantic allows for a milder European climate.

The circulation itself allows for the ocean to act as a geochemical compartment; with a complete overturning time currently on the order of around 1600 years, chemical elements or compounds introduced into the ocean are, for a time, unavailable to the atmosphere, geosphere, or cryosphere. [42]

1.1.3 Cryosphere

The cryosphere represents one of the most variable components within the climate system, encompassing the ice sheets on land and the ice shelves over the ocean. The cryosphere might be described as delicate because of how quickly its base components may change in comparison to other system elements. The northern ice sheets, being only slightly below the freezing point, are highly sensitive to temperature increases, and the resulting reduction in albedo and input of freshwater into the ocean can alter the state of both the atmosphere and the ocean. This is a main focus of this work.

1.1.4 Other Components

Naturally, the climate system is far more complex than simply atmosphere, ocean, and ice. Biology, geology, vulcanism, terrestrial roughness and orography, as well as many other components play both minor and major roles in the climate, be it on a small, regional scale, or a larger, planetary scale. While it is not the goal of this thesis to describe the precise behavior of the climate in detail based upon the interaction of each subsystem, it is important to note that any complete description of the climate system should at least consider the influence and reaction of other components as well.

1.2 RESEARCH QUESTION

The primary focus of this thesis will be on the stability and strength of the Atlantic Meridional Overturning Circulation (AMOC) and the influence of large scale ice sheet melting phenomena on this circulation. Previous studies [22, 31, 47], have suggested that this circulation may slow down or stop entirely if climate warming and increased CO_2 emissions continue to occur, leading to large amounts of ice melting and corresponding freshening of the water around the deep water

formation zones in the North Atlantic. The possible shutdown of the AMOC and retreat of Arctic ice sheets are two features of the climate system that represent a possible hysteresis with strong positive feedbacks, as well as being possible tipping points for the Earth's climate, leading to a new climate equilibrium which may be difficult to restore to a previous state [21]. It has been documented that such changes have occurred in the past as well, leading to temporarily instability of Earth's climate while the system re-stabilizes [24].

1.2.1 Potential Melting of the Greenland Ice Sheet

The Greenland Ice Sheet (GIS) represents the second largest ice sheet in the world, with approximately 2.5 million cubic kilometers of ice, about 10% of glacial ice. A complete melting of the GIS would correspond to a sea-level increase of 6.5 meters globally [7]. Many sources have documented a decrease in the GIS volume over the past several decades [3, 4, 7, 37, 52, 53]. These changes have been particularly strong in the southeast of the glacial sheet. The glacial retreat has generally been attributed to increased air and ocean temperatures, and the magnitude of melting has been reported to be increasing [7]. This observation is in stark contrast to data available regarding the GIS during the most recent glacial cycle, which suggests that the ice sheet had been generally stable [35]. Current estimates place the rate of melting for GIS to be increasing by $-30 \pm 11\,\mathrm{Gt_{ice}\,yr^{-2}}$, corresponding to a sea level increase of $0.09 \pm 0.03\,\mathrm{mm\,yr^{-2}}$. [52, 53]

Due to the fact that the GIS mass balance has been observed to have such a large range of possible values, it has been suggested that the ice sheet itself may be subject to a critical value which would trigger it to melt entirely [17], and that this melt might be irreversible [49]. The exact value of the temperature change required for melting to become irreversible has not been conclusively determined, although several groups place this value to be between 0.8-5.1 °C with 95% confidence [17]. After correcting for observed seasonal variations [4], a best estimate for such a complete melting seems to be 1.6 °C [35, 38]. The initial analyzes to create these hypothetical melting thresholds were made with regional climate models coupled to a simple ice model, such as the one by , utilizing various Greenhouse Gas (GHG) emission scenarios as presented in the IPCC report [38].

If a complete melting is possible with a relatively small degree of warming, the next natural question becomes when precisely this threshold will be reached, or if anthropogenic activity has already altered the chemical makeup of the atmosphere to induce an inevitable melting event. A commonly accepted international goal has been to limit the degree of warming to a maximum value of 2 °C, as set by the United Nations Framework Convention on Climate Change in Copenhagen in 2009. Policymakers decided that "deep cuts in global greenhouse gas emissions are required with a view to reducing global greenhouse gas emissions so as to hold the increase in global average temperature below 2 °C above pre-industrial levels" with the hopeful

effect of "preventing dangerous anthropogenic interference with the climate system" [13]. If threshold assumptions are correct, this goal of 2 °C of warming may well not be enough to prevent a melting event.

Climate change projections of when a certain average global temperature will be reached depend on the evolution of greenhouse gas emissions in the future. This is an economic phenomena, and is extremely difficult to accurately predict, since events such as the financial crisis in 2008-2009 can have noticeable impacts on emissions; although these deviations are only temporary [29]. Higher emission scenarios suggest a crossing of the 2 °C goal by 2060 [13], and regionally by as early as 2040. In those sets of scenarios that have are defined to have a "likely chance" of staying below the warming threshold (the IPCC defines 'likely' as greater than 66%), emissions would have to maximize between 2010 and 2020, with subsequent reductions to an average level of 44 Gt_{CO_2} [40]. Even if such a goal is achieved, due to physical factors such as albedo, heat capacity, and other local effects, the amount of temperature increase will be differential, with different areas warming to different degrees. As can be seen in Figure 1, even when the average global temperature is increased by 2 °C, large sections of the Arctic warm by more than this.

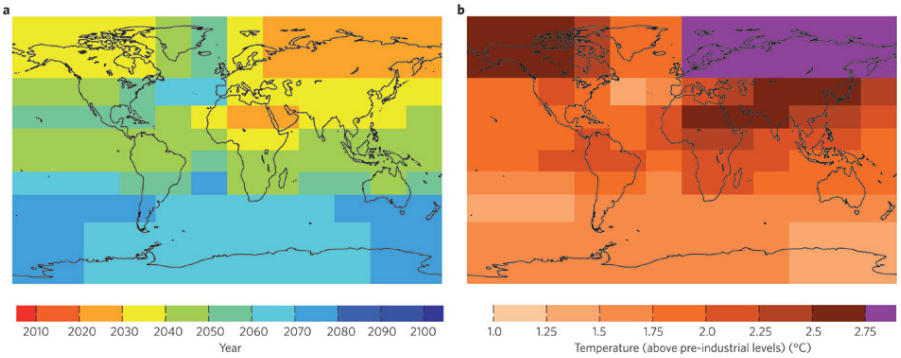

Figure 1: From Joshi et al. [13]: **a**, Median year of crossing a 2 °C threshold under the IPCC SRES A1B emissions scenario. A large part of the Northern Hemisphere is projected to experience such temperatures during the 2030s or 2040s. **b**, The expected regional temperatures when global average temperature reaches 2 °C. The spatial patterns are non-uniform.

Considering that the 2 °C goal has probably already been overshot [25], and that the threshold temperature increase for a complete melting of the GIS has also already been exceeded, the next question becomes what this implies for the global climate and what sort of changes can be expected. Of primary concern are the deep water formation zones directly adjacent to Greenland, as these will very likely be affected by a large injection of freshwater.

1.2.2 Deep Ocean Circulation Instability

The North Atlantic ocean is one of two sites of deep water formation in the modern ocean, and therefore is a fundamental feature in

Thermohaline Circulation (THC). It has by now been well established that deep ocean circulation contributes greatly to the heat distribution of the Northern Atlantic [31], warming the eastern seaboard of the United States and many of the coastal countries of western Europe by several degrees. Additionally, it is known that the system reacts to changes in the freshwater input [30]. How sensitive the THC system is to varying amounts of freshwater input has not yet been determined conclusively, and the system's nonlinear nature could cause deep water circulation to switch to a new equilibrium, suggesting a bi-stable or possible multi-stable climate system feature. Bi-stability implies the overturning strength can change with respect to freshwater input, settling into a new steady state that does not return to the initial strength if the freshwater input were to be removed.

The sensitivity is possibly due to the complexity of the formation process for North Atlantic Deep Water (NADW). An interaction of wind driven surface circulation, temperature change as water cools near the polar region, and increases in salinity due to brine injection by forming sea ice all contribute to the formation of NADW [18]. It is additionally possible to transport a salinity change towards a downwelling region from the South Atlantic [6]. While it is possible to break down the deep water formation into a conglomerate of various smaller water packets interacting on an eddy scale [42], the overall principle remains the same - deep water sinks due to an increase in density caused by modifying the water packets temperature and salinity, and a large injection of freshwater due to ice sheet melting would alter the amount by which the density is changed.

A previous study has shown that the Thermohaline Circulation may respond to changes in atmospheric concentrations of carbon dioxide alone, with a shutdown occurring after a critical GHG concentration is reached [47]. The mechanism involved here is connected to the overall formation process of deep water: In order for a water mass to sink, it must obtain a certain critical density. Since a higher amount of carbon dioxide in the atmosphere directly leads to an increase in ocean surface temperature, the amount of deep water that can be formed simply by increasing the salinity decreases. The warm water floats, decreasing the density of the water mass, therefore requiring additional salt to overcome the density gradient. If no additional source of salt is available, the formation rate of deep water is impacted. This not only has implications for the heat transport between the equator and the poles, but would also modify the ability of the ocean to take up and store excess carbon dioxide from the atmosphere, assuming the system remains in disequilibrium, with more CO_2 in the atmosphere than in the ocean. The additional influence of meltwater suggests that the continued behavior of the THC system in its current state is in danger.

Rapid climate change between various stable states is certainly not a new concept, and the possibility of various natural triggers continues to be an active area of paleoclimate research [5, 41, 46]. The thermohaline system has exhibited a variety of equilibria in the past, between an extreme of no circulation, to the existence of several deep

water formation zones [31]. In the past, these stable states have also been influenced by meltwater, temperature changes, and sea ice cover. Since these sort of changes are expected to occur due to an increase in GHG concentration, the potential for abrupt climate change also exists in the future.a

1.2.3 Climate Consequences

Were a shutdown of THC to occur, several changes to the surface climate could be triggered. While the degree of the effects is still under debate, several consequences are agreed upon: the average yearly temperature for regions adjacent to the Northern Atlantic would decrease by 1 to 9 degrees, with a winter decrease of 2 to 13 degrees [15]. Precipitation changes are also excepted, although it is unclear if this will be a wetting or drying. Overall, the hydrologic cycle could weaken, as well as induce a change in the frequency and strength of storms and extreme weather events in the Northern Atlantic. A summary by Zickfeld et al. [56] of possible consequences of weakening or shutdown of the AMOC is presented in Table 1

Unfortunately, due to the large number of uncertainties and the chaotic nature of the climate system, it is difficult to accurately predict where, when, and to what extent which of these effects may occur. However, it is evident that an adjustment of the AMOC would dramatically influence the climate in the Northern Atlantic region with consequences spreading to the rest of the global climate as well.

1.3 APPROACH

In the past, studies on the sensitivity of the AMOC system to freshwater perturbations have been preformed using a method known as "hosing". [33] In this technique, a prescribed amount of freshwater is added to the North Atlantic. Alternatively, a specified amount of salt is removed. This results in a change of the salt budget, and a shift of the THC system to a different state. Unfortunately, these types of experiments must work with estimates regarding the amount of freshwater that should be applied. The novelty of the work presented here is the dynamic nature of the ice sheet component.

While the description of the experiments to be preformed as well as an explanation of the models is saved for the next chapter, the general approach used to address the research question is as follows: A coupled ocean-atmosphere-ice model, incorporating both Greenland and Antarctica, will be perturbed with reasonable approximations of possible GHG emissions. Since the ice model is dynamic, the exact extent to which GIS may melt will be evident, and the impacts on the ocean system and the overall climate of the North Atlantic region will then be analyzed.

Table 1: Potential consequences of AMOC weakening in the North Atlantic and Globally

North Atlantic	Global
Weakening of hydrological cycle	Shift in tropical precipitation patterns
Change towards Pacific type of climate	Change in intensity of Monsoons
Progression of sea ice	Warming in Tropical Atlantic and South Atlantic
Shift of oceanic fronts	Increase in hurricane activity in Tropical Atlantic and South Atlantic
Shift of storm tracks	Cooling of Northern Hemisphere
Increase in extreme cold events	Change in atmospheric standing waves
Impacts on fisheries and fish-farming	Changes in large-scale atmospheric circulation
Impacts on marine and terrestrial ecosystems	Changes in sea ice extent in Southern Ocean
Impacts on water transportation	Changes in oxygen ventilation
Higher probability of storm surges	Reduction in oceanic carbon uptake

2 EXPERIMENTAL SETUP AND MODEL DESCRIPTION

2.1 EXPERIMENTS

In order to examine the effects of increased greenhouse gas levels in possible future climates, a series of modeling experiments will be preformed with a dynamic climate model consisting of an atmospheric component, an ocean component, and an ice component. Each module contains a full set of physics, both motion based of fluid dynamics and thermodynamics, and can exchange information regarding mass and energy conservation with the others over a coupling program. The greenhouse gas levels considered are based on the IPCC's RCP scenarios, with the goal of approximating a subset of various reasonable evolutions of atmospheric composition altered by socioeconomic and developmental changes.

2.1.1 Greenhouse Scenarios Considered

In order to ensure this work is comparable to previous studies, two different ending GHG levels were chosen. The IPCC's Representative Concentration Pathway (RCP) Scenarios 4.5 and 6 have an atmospheric greenhouse gas concentration designed to generate a $4.5\,W\,m^{-2}$ and $6\,W\,m^{-2}$ increase by the end of 2100, respectively. These are different from previous scenarios that prescribe a direct amount of GHG to be emitted. Rather, multiple climate factors that may contribute to an alteration of the climate forcing are considered; for instance, aerosols in the atmosphere or anthropogenic mitigation, allowing for better interaction between various disciplines interested in climate projections [27]. These various changes are cumulatively equated to a reasonable, albeit estimated, change in CO_2

After the initial paper published to introduce scenario 4.5, Thomson et al. [48] describe the scenario: "RCP4.5 is a scenario of long-term, global emissions of greenhouse gases, short-lived species, and land-use-land-cover which stabilizes radiative forcing at $4.5\,W\,m^{-2}$ (approximately 650 ppm CO_2-equivalent) in the year 2100 without ever exceeding that value." RCP 4.5 considers the possibility of climate policies functioning to limit emissions.

RCP 6 is defined very similarly: "RCP6 is a scenario of long-term, global emissions of greenhouse gases, short-lived species, and land-use/land-cover change which stabilizes radiative forcing at $6\,W\,m^{-2}$ in the year 2100 without exceeding that value in prior years" [23]. The CO_2 equivalent concentration is 855 ppm assuming a climate sensitivity of 3.0, which would result in a 4.9 °C average temperature increase.

The equilibrium concentrations for GHG forcings are slightly different than those reported in the initial scenario development, and those used in the Coupled Model Intercomparison Project 5 (CMIP5) by the IPCC are the ones that will be used. For RCP 4.5, the final concentration is about 583 ppm of GHG, and for RCP 6, it is 808 ppm of GHG [26].

2.1.2 Possible Emission Schemes

In order to examine a broad range of emission schemes to reach these levels, 3 different emission rates will be considered, based upon a similar emission variability presented in Stocker's study on carbon dioxide emissions rates and the effect on AMOC strength [47]. The atmospheric GHG concentration (in CO_2 equiv) will be increased once in a set of "slow" scenarios with 0.5% growth per year, once at a "medium" rate with 1% per year, and once at a "fast" rate at 2% per year. This allows for 6 different emissions tracks to be examined: RCP4.5s, RCP4.5m, RCP4.5f, RCP6s, RCP6m, RCP6f. Experiments are summarized in Table 2 as well as in Figure 2

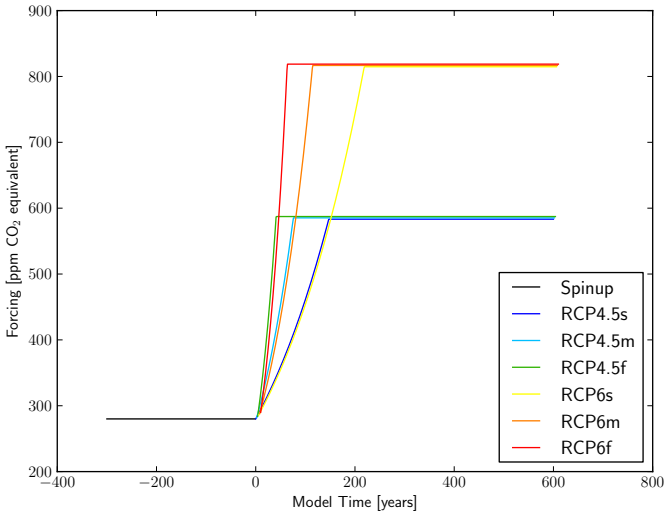

Figure 2: Emission levels and ramping speeds considering in the experiments. A spinup time of approximately 3000 years at a CO_2 equivalent of 280 ppm was used to equilibrate the model internally before any new forcings were applied. The slight offset seen in the curves was introduced to be able to distinguish overlapping concentrations.

2.1.3 Coupling Variations

One of the key limitations of the initial modeling experiments that this project is based on was inadequate computing power. As such, a very simple model was used to construct the initial findings provided by Stocker and Schmittner [47]. Apart from the clear improvements to

Table 2: Experiments Performed

Scenario Basis	GHG Level [ppm]	Ramping [a]	Ice Sheets	Code
RCP 4.5	583.287	148	Dynamic	4.5s
		75	Dynamic	4.5m
		38	Dynamic	4.5f
RCP 6	808.709	213	Dynamic	6s
		107	Dynamic	6m
		54	Dynamic	6f
RCP 4.5	583.287	148	Off	4.5s-ni
		75	Off	4.5m-ni
		38	Off	4.5f-ni
RCP 6	808.709	213	Off	6s-ni
		107	Off	6m-ni
		54	Off	6f-ni

the dynamic atmosphere and ocean models, one additional enhancement that will be made here is the inclusion of an ice component, and in order to demonstrate the effects of including this component, two experiment suites will be run. The first will have a fixed ice component, running only dynamic atmosphere and ocean components. While a decrease in the AMOC is still likely, it will probably be amplified in the case with a dynamic ice module. Running both sets of experiments (one with and one without dynamic ice) will also allow for a demonstration of the significance of including a well-developed ice model.

While it is possible to include other components as well - land vegetation via JSBACH and ocean biogeochemistry HAMOCC, and while the effects of a GIS melt and AMOC slowdown are certainly interesting on these components, the addition of these modules greatly increases the model run time. Due to time constraints and the technical development of the coupled model system at the time, an examination of changes in ocean biogeochemistry and land vegetation due to climate shifts are not included in the scope of this project.

2.2 OUTPUT EVALUATION

Several results are achieved by this series of experiments. As discussed in the previous chapter, changes in the Arctic region have

impacts both on the GIS and AMOC. The variation in CO_2 emission pathways should provide information about a melting threshold, and if one exists, to what extend the GIS will melt. Additionally, the progression of the AMOC strength will be shown, and it may be possible to see a new equilibrium form, or a complete shutdown may occur. Finally, using output from the atmospheric model, changes in the surface conditions will be shown, demonstrating what a slowdown of the AMOC and melting of the GIS may imply for the regional climates around the Atlantic. It is of particular interest to see if the timing and amount of GHG emissions has an impact on any of these results, be it in the timing or in the extent of the result itself.

2.3 COSMOS GENERAL CIRCULATION MODEL

What follows is a general description of the various components used in the model of this study. The modeling work was completed using the COSMOS Climate Model developed at the Max Plank Institute for Meteorology in Hamburg. COSMOS is an Earth System Model (ESM) which takes into account physical knowledge of the atmosphere, ocean, and cryosphere; and allows for a coupling scheme between them which can account for physical and chemical interactions that may occur. This allows for a fairly sophisticated representation of planetary climate; and while drawbacks naturally exist, these will be discussed later in the Conclusion, section 6.3.

The governing numerical equations for each model are briefly presented with an explanation of the terms involved, as well as any other calculations made by the model. It is of particular interest to examine the assumptions that the model must make, some of the parameterizations are truncated representations of reality, simplified so that the equations may fit into the discretized spatial and temporal grid of the model. These descriptions are based primarily on the model handbooks, which provide a far more detailed description of the model's internal workings. URLs to these handbooks are additionally given in the references.

2.3.1 ECHAM5

The model description here is based primarily on the MPI-Meterology Institute's report and documentation for ECHAM5. A full derivation of the governing physics equations is not included and can be viewed in the ECHAM5 description by Roeckner [39].

The ECHAM5 component describes the atmosphere. Based upon a spectral representation of various prognostic variables (such as Vorticity ξ, Divergence D, Temperature T, Pressure $\ln p_s$ among many others), ECHAM5 includes a full set of atmospheric dynamics with resolutions up to T159[1], corresponding to 480 longitudes and 240 lat-

1 This represents the amount of truncations allowed in a wave representation of the variable

itudes. The implementation of ECHAM5 used in this study uses 96 longitudes and 48 latitudes, corresponding to a T31 resolution. 19 vertical levels are also included.

The grid size necessitates certain physical processes to be parameterized in order to approximate their behavior over an entire grid space, since the scale of the phenomena is either spatially or temporally too small to be directly calculated. Processes such as advection, horizontal and vertical diffusion, various heat and water budgets, subscale orography, and various cloud microphysics are all described in the model in a parameterized form.

One of the more important aspects for this study is how the model will resolve albedo, a parameter which certainly has a feedback on the entire climate system, and one that will be altered should a large scale melt occur. ECHAM5 allows for an annual mean background albedo over snow-free surfaces, defined as α_{bg}. This background value stems from satellite measurements. For snow and ice surfaces, ECHAM5 assumes a linear dependence of albedo on surface temperature. Values are allowed between a predefined melting point $T_s = T_0$ to a maximum value, $T_s \leqslant T_0 - T_d$. The albedo of a snow covered area therefore is:

$$\alpha_{sn} = \alpha_{sn,min} + (\alpha_{sn,max} - \alpha_{sn,min}) f(T_s)$$

where

$$f(T_s) = \min \left\{ \max \left[\left(\frac{T_0 - T_s}{T_0 - T_d} \right), 0 \right], 1 \right\}$$

where T_d represents a temperature for a specific surface type. Based upon this, ECHAM5 can distinguish several different surface albedos: land, canopy, land ice, sea ice, lake ice, and snow on lake ice.

Additional surface processes are also modeled, and while not relevant to the direct question of this study, are included for a complete model description. ECHAM5 can also calculate head budget from the soil, water budget (both rain and snow) at the canopy, at the surface, and in the soil; includes a component for describing the temperature, albedo, ice cover and ice thickness thickness of lakes, and has the ability to determine sea surface temperature in order to couple to a mixed layer ocean, where the upper layers of the ocean model are interactive and exchange information with the atmosphere.

2.3.2 MPI-OM

The oceanic component of COSMOS used is the Max Planck Institute Ocean Model (MPI-OM). It is a general ocean circulation model drawing upon basic equations and has the ability to represent thermodynamic processes. Spatially, the model can solve small, eddy scale processes as well as larger motions on the gyre scale, with the subscale limit lying at around 1 kilometer. [55] Which of these processes are included in the analysis depends on the resolution selected at the beginning of the experiment.

Ocean primitive equations are used to describe horizontal momentum balance for a hydrostatic Boussinesq fluid[2] in a rotating spherical reference frame, acting as a primary driving force for the model:

$$\frac{d\vec{v_o}}{dt} + f(\vec{k} \times \vec{v_o}) = -\frac{1}{\rho_w}\left[\vec{\nabla}_H (p + \rho_w g\zeta)\right] + \vec{F_H} + \vec{F_V}$$

where $\frac{d\vec{v_o}}{dt}$ is the ocean horizontal velocity vector, t is time, f is the Coriolis parameter, $\vec{k}$ is a unit vector orthogonal to the ocean's surface. ρ_w represents a constant reference pressure, $\vec{\nabla}_H$ is the horizontal gradient operator of internal pressure p, density ρ_w, gravity g, and sea surface height ζ. $\vec{F_H}$ and $\vec{F_V}$ represent parameterized forms of horizontal and vertical eddy viscosity. These are parameterized due to grid size limitations.

The formulation $f(\vec{k} \times \vec{v_o})$ is a combination of the two Coriolis terms, and can be rewritten in the more familiar form:

$$\frac{du}{dt} - fv = \frac{\partial \Phi}{\partial x} + \nu_h \nabla_h^2 u + \nu_v \frac{\partial^2 u}{\partial z^2}$$
$$\frac{dv}{dt} + fu = \frac{\partial \Phi}{\partial y} + \nu_h \nabla_h^2 v + \nu_v \frac{\partial^2 v}{\partial z^2}$$

$\nu_h \nabla_h^2 u$ and $\nu_v \frac{\partial^2 u}{\partial z^2}$ (and the v equivalents) are the turbulent terms which are parametrized in the model.

Pressure follows the hydrostatic equation $\frac{\partial p}{\partial z} = -g\rho$, and under the assumption of an incompressible ocean, the velocity terms follow from an integration over the depth of the ocean for the time change of the surface elevation ζ:

$$\frac{\partial \zeta}{\partial t} = w_o|_{z=\zeta}$$
$$\frac{\partial w_o}{\partial z} = -\vec{\nabla}_H \cdot \vec{v_o}$$
$$w_o|_{z=\zeta} = -\vec{\nabla}_H \cdot \int_{-H}^{\zeta} \vec{v_o}\, dz$$

Potential temperature θ[3] and salinity S are subject to advection and diffusion, although these processes are parameterized for horizontal and vertical diffusion due to the sub-scale nature. Several other processes and properties must be parameterized, such as viscosity, diffusivity, eddy-generated mixing phenomena, as well as convection. Slope convection is one of the physical backgrounds to thermohaline circulation progression. It describes how deep water packets will move once they have already sunk, is not well resolved in the MPI-OM due to the coarse z spacing; a problem which is fixed with a bottom boundary layer parameterization.

2 In buoyancy driven flow, states that differences in density are sufficiently small to be neglected unless the density term has a factor of g.

3 Potential temperature θ is the temperature a parcel of water would have if it were brought adiabatically to some predefined reference pressure.

MPI-OM also includes a sea ice subcomponent. The dynamics are based upon a two dimensional momentum balance:

$$\frac{d\vec{v_i}}{dt} + f(\vec{k}) = -g\vec{\nabla}\zeta + \frac{\vec{\tau_a}}{\rho_i h_i} + \frac{\vec{\tau_o}}{\rho_i h_i} + \vec{\nabla} \cdot \sigma_{mn}$$

with: f - corliolis parameter, $\vec{k}$ - unit vector normal to the Earth's surface, ζ - sea surface elevation, g - gravitational acceleration, t - time, h_i - ice thickness, ρ_i - ice density, $\vec{v_i}$ - ice velocity due to wind and ocean stress, τ_a - wind stress, τ_o - ocean stress, σ_{mn} - internal stress of ice.

MPI-OM is also able to calculate thermodynamic properties of ice, allowing for melting and freezing processes. Due to the sub-scale nature of some of the processes involved in melting and freezing, many of the terms are parameterized. The conductive heat flux with available heat for phase transitions can be described via a zero-layer formulation:

$$Q_{cond} = k_i \frac{T_{freeze} - T_{surface}}{h_i}$$

with k_i as the thermal conductivity, T_{freeze} as the freezing temperature of saline water, and h_i is the effective thickness of the ice/snow layer. At temperatures above the freezing point, energy is transferred into the latent energy term to allow for ice melting and is otherwise used to warm the entire layer to a new temperature.

The final aspect of the sea ice subcomponent is the ability to calculate brine rejection, allowing for the consideration of fresh and salt water exchanges during sea ice growth and melt processes. The sea ice of MPI-OM is assumed to have a constant, age-independent salinity of 5 psu. The upper layer of the ocean, with salinity S_1 is allowed to change by an amount ΔS according to ice growth and snowfall:

$$(S_1 + \Delta S)\Delta z'^{old} + \frac{\rho_i h_i^{old}}{\rho_w} S_{ice} = S_1 \Delta z'^{new} + \frac{\rho_i h_i^{new}}{\rho_w} S_{ice}$$

with δz being the upper ocean layer thickness before and after a growth or melting event, and h being either the new or old amount of sea ice. ρ designates the density of water or ice.

2.3.3 RIMBAY

RIMBAY is a dynamic Ice Sheet Model (ISM) with the ability to calculate ice sheet dynamics not only based upon approximations, but also allows for the integration of higher order equations when considering stresses (Full Stokes equation). The ability to use both approximations and more precise calculations has the advantage of increasing the model accuracy without necessarily sacrificing computing time. Additionally, RIMBAY implements moving margins to simulate sheet-shelf boundaries, ice-ocean boundaries, and ice-rock boundaries, allowing for the simulation of events such as iceberg calving and glacial retreat. For the model studies presented here, the Stokes equation can be simplified by two approximations:

SHALLOW SHELF APPROXIMATION Initially developed by MacAyeal in 1989 the Shallow Shelf Approximation (SSA) reduces the full Stokes:

$$\begin{aligned}
\frac{\partial \tau_{xx}}{\partial x} + \frac{\partial \tau_{xy}}{\partial y} + \frac{\partial \tau_{xz}}{\partial z} &= \frac{\partial p}{\partial x} \\
\frac{\partial \tau_{xy}}{\partial x} + \frac{\partial \tau_{yy}}{\partial y} + \frac{\partial \tau_{yz}}{\partial z} &= \frac{\partial p}{\partial y} \\
\frac{\partial \tau_{xz}}{\partial x} + \frac{\partial \tau_{yz}}{\partial y} + \frac{\partial \tau_{zz}}{\partial z} &= \frac{\partial p}{\partial z} + \rho g
\end{aligned}$$

to

$$\begin{aligned}
\frac{\partial \tau_{xx}}{\partial x} + \frac{\partial \tau_{xy}}{\partial y} + \frac{\partial \tau_{xz}}{\partial z} &= \frac{\partial p}{\partial x} \\
\frac{\partial \tau_{xy}}{\partial x} + \frac{\partial \tau_{yy}}{\partial y} + \frac{\partial \tau_{yz}}{\partial z} &= \frac{\partial p}{\partial y} \\
\cancel{\frac{\partial \tau_{xz}}{\partial x}} + \cancel{\frac{\partial \tau_{yz}}{\partial y}} + \frac{\partial \tau_{zz}}{\partial z} &= \frac{\partial p}{\partial z} + \rho g
\end{aligned}$$

In this case horizontal strain rates are balanced only by horizontal stresses, since the assumption is that vertical shear stresses are small enough to be neglected. The primary restriction is that the thickness is much smaller than the horizontal extent. This approximation is only applied to shelf ice. While still being attached to the continental ice sheet, shelf ice is a distinct component floating on the ocean. While nature allows for an ocean-ice interaction surface here, the model development at the time of this study was at a stage where such an interaction was not yet implemented.

SHALLOW ICE APPROXIMATION The Shallow Ice Approximation (SIA) goes one step further and assumes that the gradients of sheer stresses are only determined by a vertical component. The full set of Stokes equations thus becomes:

$$\begin{aligned}
\cancel{\frac{\partial \tau_{xx}}{\partial x}} + \cancel{\frac{\partial \tau_{xy}}{\partial y}} + \frac{\partial \tau_{xz}}{\partial z} &= \frac{\partial p}{\partial x} \\
\cancel{\frac{\partial \tau_{xy}}{\partial x}} + \cancel{\frac{\partial \tau_{yy}}{\partial y}} + \frac{\partial \tau_{yz}}{\partial z} &= \frac{\partial p}{\partial y} \\
\cancel{\frac{\partial \tau_{xz}}{\partial x}} + \cancel{\frac{\partial \tau_{yz}}{\partial y}} + \cancel{\frac{\partial \tau_{zz}}{\partial z}} &= \frac{\partial p}{\partial z} + \rho g
\end{aligned}$$

The SIA is justifiably applicable if the horizontal span is much larger than the typical thickness, which is the case for the larger ice sheets included in an ESM-ISM coupled system.

While RIMBAY is able to implement and solve the full Stokes equations to describe the internal continuum mechanics of an ice sheet, in order to speed up computation times, several reductions were made:

1. `rimbay` was implemented with the SIA, with the justification that the ice sheets included in the model were large enough that the amount of additional information gained by using full Stokes as opposed to an approximation was minimal. The technical development of the model did not allow for the inclusion of shelf ice.

2. The ice sheet's grounding line remained fix after the spin up, primarily due to the technical state of the development at the time of the experiment. This had some implications for how the model is able to treat freshwater fluxes, which will be discussed in the conclusions.

Several inputs are initially required in order to construct an ice sheet model: information regarding the bedrock elevation, geothermal heat flux, and initial ice distribution are all important for generating an ice sheet. So far, it has been possible to model both Greenland and Antarctica. Although other, smaller glaciers (such as inland ones) can also be simulated, the information gained by this small scale simulation is not particularly useful for the problem addressed here as well as introducing a significant increase in the computation time. The inputs remained fixed for the entire experiment, and are shown in Figure 3

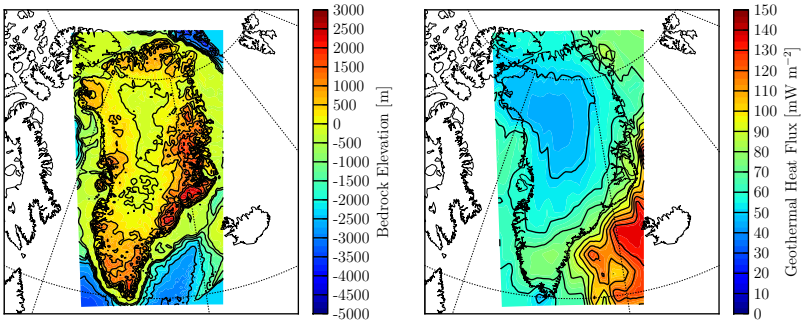

Figure 3: Input fields required by RIMBAY, not including the inputs received from the atmosphere module.

The information for geothermal heat flux were taken from published values [43], along with data for the bedrock topography and initial ice distribution from the AlbMap project [20] for Antarctica and measurements taken by Bamber et al. [1] for Greenland. The datasets for both ice sheets were provided on a 5 km resolution, although this was interpolated to a 20 km model grid to improve computation time while still retaining the required accuracy.

2.4 DOWNSCALING & COUPLING RIMBAY TO COSMOS

RIMBAY couples to COSMOS, exchanging certain variables in order to allow each component of the coupled model to adapt to changes in the other. From observations, it becomes clear that processes at work in the atmosphere, the ocean, or the cryosphere operate at very different time scales, requiring different time steps for each component. The atmosphere, for example, should be calculated on a finer temporal resolution to preserve realistic behavior, whereas ice sheets require decades or centuries to respond to changes. This leads to the previously accepted first approximation that we can consider ice sheets with generally static behavior for a majority of climate projections, although recent studies suggest that it is indeed important to consider ice sheets dynamically [12].

Depending on the time scale of the model run and the predicted changes, 2 types of information exchange can be implemented: Synchronous, or transient coupling, allows both models to run in parallel, exchanging information on an equal time scale (1 year atmosphere-ocean for every 1 year ice sheet). It is also possible to couple the two models asynchronously, maintaining an essentially stable ice sheet state while other, quicker climate components react before recouping the two. This approach, however, is not applicable to the experiments described here, as the ice sheet is predicted to melt on a fairly rapid time scale. The coupling preserves the freshwater budget, exchanging differences in the calving rate, albedo, and geopotential. RIMBAY also receives several fields from COSMOS during the coupling - atmospheric parameters such as snow accumulation and mean temperatures are pushed to RIMBAY. The setup can be seen in the schematic shown in Figure 4

When examining the grid resolution of the components, the necessity to apply some form of downscaling to the ice sheet becomes clear, since directly taking the coupled variables as given by ECHAM5 results in unrealistic, coarse distributions. Three fields in particular need to be resized and interpolated; net snow accumulation, snow melt, and surface temperature. Table 3 summarizes the variables exchanged. A field average of both 2 meter surface temperature and net precipitation as seen by the ice sheet for the entire set of experiments is shown below in Fig. 5

The coupling and downscaling process, developed by Barbi et al. [2], employs a variation of inverse distance weighting based upon the Shepard algorithm [44]. In general, finding a specific interpolated value u for a given point $\mathbf{x}$, the interpolating function used is:

$$u(\mathbf{x}) = \sum_{i=0}^{N} \frac{w_i(\mathbf{x}) u_i}{\sum_{j=0}^{N} w_j(\mathbf{x})}$$

with

$$w_i(\mathbf{x}) = \frac{1}{d(\mathbf{x}, \mathbf{x_i})^p}$$

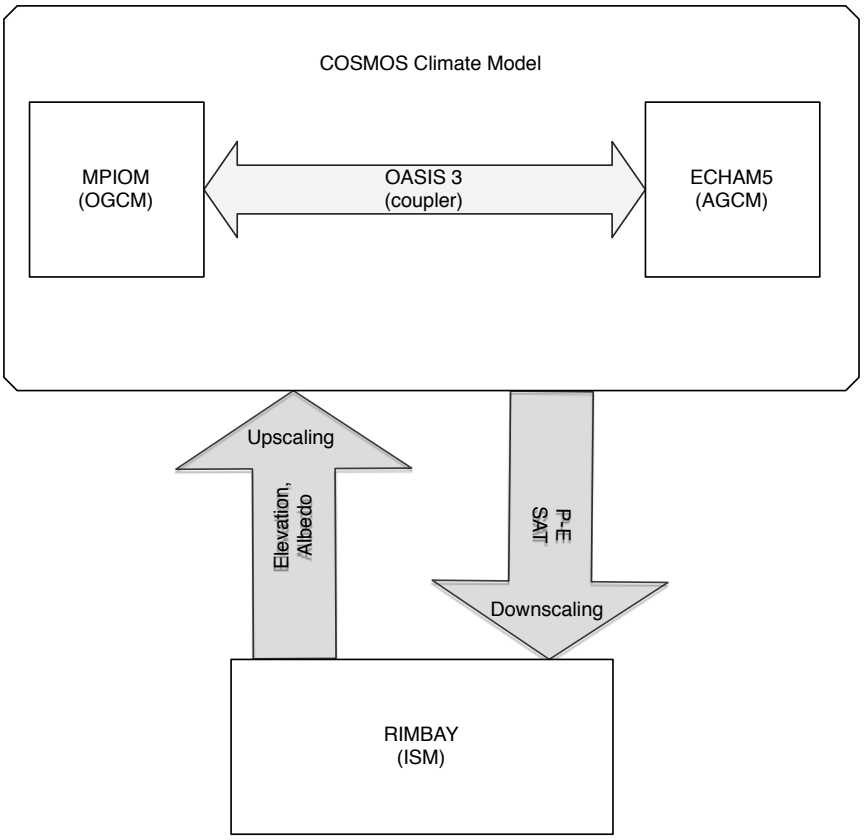

Figure 4: Model Schematic

Table 3: Data exchanged between RIMBAY and COSMOS

RIMBAY → COSMOS	**RIMBAY ← COSMOS**
Calving Rate	Net Snow Accumulation
Geopotential Height	Net Ablation
Albedo	Mean Surface Temperature

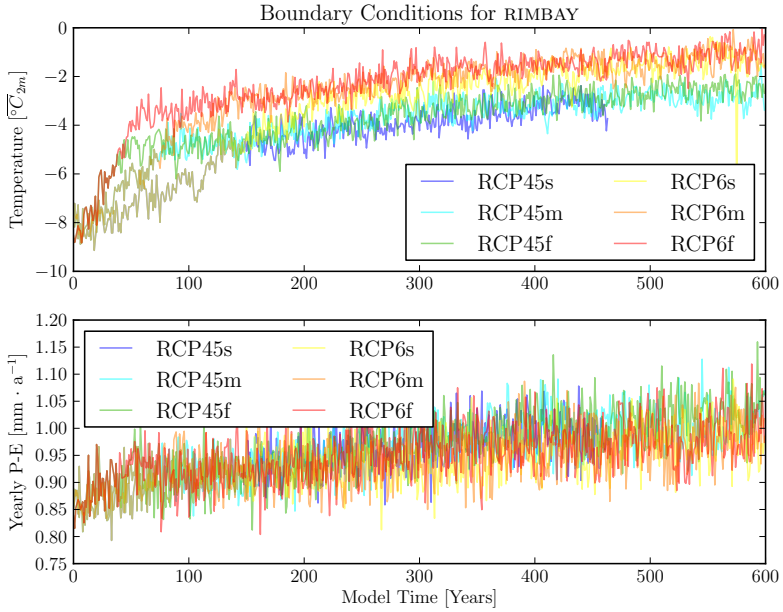

Figure 5: Input fields required by RIMBAY received from the atmosphere module.

x denote an interpolated value, $\mathbf{x_i}$ an known point, **d** is the distance between the two, and N is the total number of points that are known. The power parameter p was chosen as 2.7. Figure 6, taken from Barbi et al. [2], shows the significance of including a downscaling routine. As can be seen, the ice sheet is very sensitive to the difference in resolution used.

The coupling procedure, while allowing the system to gain more realistic information about ice sheets is not without limitations. One significant drawback of the RIMBAY model is its inability to influence orography as well as static ice-sea and land-sea masks. This means that any melt water generated by RIMBAY will not have an impact on the sea level, which is realistically expected to rise during large-scale melting events. Additionally, calving only occurs over the grounding line – the interface between ice-free bedrock and the ice sheet – which is not allowed to migrate in this implementation of the ice sheet model. In nature, as an ice sheet melts, the grounding line will also retreat, suggesting that the amount of freshwater input as simulated by this coupling method may be incomplete.[4]

4 This specific problem is discussed further in the conclusions.

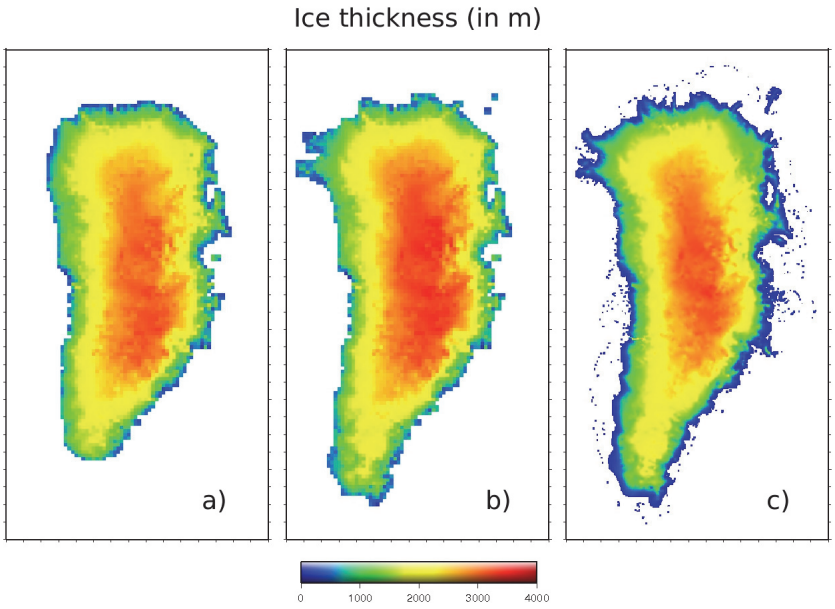

Figure 6: From Barbi et al. [2]: Ice thickness of the Greenland ice sheet before (a) and after (b) the downscaling produce, after 10000 ice model years. This is compared to measured data (c, Bamber et al., 2001)

3 RESULTS: GLOBAL CLIMATE DATA

In the following chapter, the output of the various simulated climate components will be presented. An emphasis shall be placed on highlighting differences between the two model setups.

This will serve as the description of the background climate state of the atmosphere, the ocean, and the ice sheets, before detailed analysis of the changes to the North Atlantic freshwater balance and the AMOC changes resulting from this modified balance will be presented.

3.1 ATMOSPHERIC COMPONENT ECHAM5

As has been documented before with the RCP Scenarios used in this work [23, 26, 48], the atmosphere experiences an overall warming in all experiments, accompanied by an intensification of the hydrological cycle. The primary focus of this section will be the impact of the atmosphere on possible freshwater fluxes into the ocean, both via overall warming, which could contribute to melting, and by examining the precipitation patterns within the atmosphere. Also, a change in the albedo will be shown, as this will possibly enhance other changes.

3.1.1 Atmospheric Warming

Introducing the coupled ice sheet model has an overall cooling effect on the entire climate, which acts to counter the warming caused by the GHG increase. In order to demonstrate that this is statistically significant, several representations shall be used. To begin, spatial patterns of the relative temperature increases at the end of the experiments as well as the anomalies of these temperatures to the other model setup are presented.[1] Following this, scatter plots of possible temperatures found across all latitudes are shown, again with both model setups in order to highlight the difference between the two. Lastly, time series of the 2 meter global mean atmospheric temperature are presented.

From the spatial distribution shown here it is clear that a strong polar amplification is present at both CO_2 concentrations. The changes based upon model configuration is strongest where the ice sheet models are incorporated. The fact that the climate model without dynamic

1 In order to conserve space, only the experiments RCP6m and RCP4.5m, corresponding to a 1% increase in GHG per year are show unless the effect of changes in speed are to be demonstrated. The other experiments can be found in the appendix.

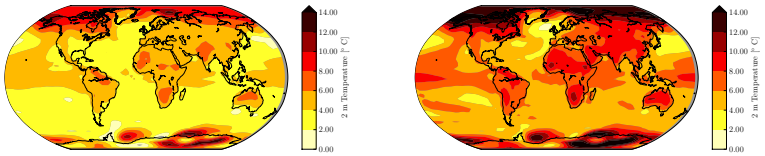

(a) RCP 4.5 1% `aoi` anomaly to control state

(b) RCP 6 1% `aoi` anomaly to control state

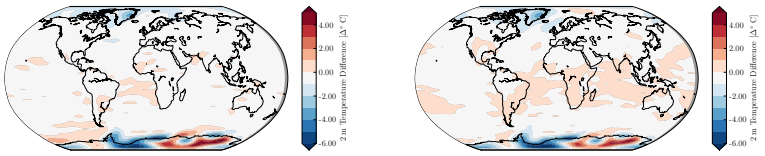

(c) RCP 4.5 1.0% `aoi - ao`

(d) RCP 6 1.0% `aoi - ao`

Figure 7: The differences between the end of the simulation run and the control state are shown (a & b), as well as the differences between the model configurations (c & d). It should be noted that positive values in the configuration comparisons imply that the `ao` (atmosphere-ocean) version simulates a warmer atmosphere, while negative values indicate that the `aoi` (atmosphere-ocean-ice) version simulates a warmer value. All datasets are 30 year climatological means.

ice sheets generates a warmer atmosphere is likely due to the fact that latent heat is taken from the atmosphere to melt the ice.

The polar amplification is explainable via a simple feedback mechanism. As both forcing scenarios will cause the atmosphere to heat up, the average annual snow and sea ice cover will retreat, reducing albedo, and allowing the system to take up more solar energy, thereby enhancing the warming.

In Figure 8, the overall heating from Figure 7 is seen once more, this time split up by latitude. The orange color represents RCP6 whereas the light blue represents RCP4.5[2]. The inclusion of a dynamic ice sheet has a marked cooling effect at every latitude. To demonstrate this, the absolute value of the temperature differences between model configurations is shown in the lower left panel, where each point represents a zonal average comprised of 96 simulated values available for each latitude. These differences fall well below the 1% significance level, as seen from the P-Values in lower right panel, suggesting that the cooling introduced by RIMBAY, while most pronounced at those latitudes that include a dynamic ice sheet, is also present at mid latitudes. The comparison made here operates under the null hypothesis that all possible temperatures within a zonal band would have an average difference of 0 when examining the configuration with and without dynamic ice sheets.

Lastly, a time series of the global mean 2 meter atmospheric temperature is presented, Figure 9. The cooling effect is once again evident. In order to examine what exactly may be causing this cooling effect, the differences in the albedo between the two models is examined in the next section.

3.1.2 Albedo Changes

One of the primary climate feedbacks generated by overall warming is a reduction of planetary albedo, due to the retreat of the ice caps as well as the reduction of sea ice cover, particularly during the summers. While both model configurations simulate changes in the sea ice, only the configuration with dynamic ice sheets has the ability to calculate changes in albedo due to reduction of the Greenland Ice Sheet, as well as changes in albedo caused by modifying conditions in the Southern Ocean due to the introduction of a dynamic Antarctic Ice Sheet. While the actual changes to the ice sheets will be presented later, a time series of global yearly average is shown here, as well as a spatial plot of albedo anomalies to the control state. Anomalies between the two model configurations are also shown in order to demonstrate where exactly the ice sheet inclusion is impacting the overall system.

From Figure 10, it can be seen that a slightly larger albedo is simulated when including the ice sheet. This is caused by sea ice stratification, as the cooling around the ice sheet allows thicker sea ice to form. Since more incoming radiation is reflected in this case, the overall temperature is expected to decrease, partially explaining the changes

2 See appendix notes for a breakdown of colors used for each experiment

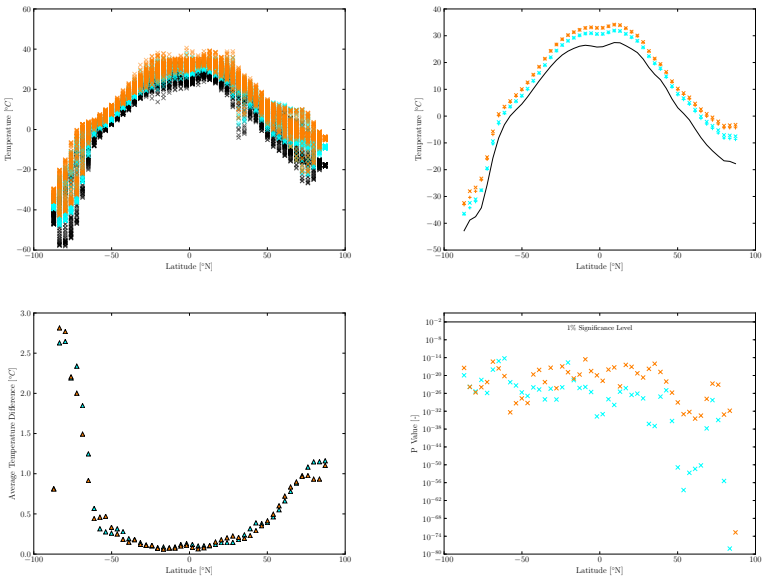

Figure 8: Various representations of the statistics of including a dynamic ice sheet model. The upper left panel show the absolute temperatures for each longitude at the end of the simulation at every possible latitude, with the longitudinal averages for each latitude are shown in the upper right. The lower left panel show the differences of the model configuration, demonstrating that there is a fairly large difference generated by introducing the ice sheet model, which has a very high level of statistical significance as shown by the P-Values plotted in the lower right. The orange colors represent RCP6, whereas the blue ones represent RCP4.5

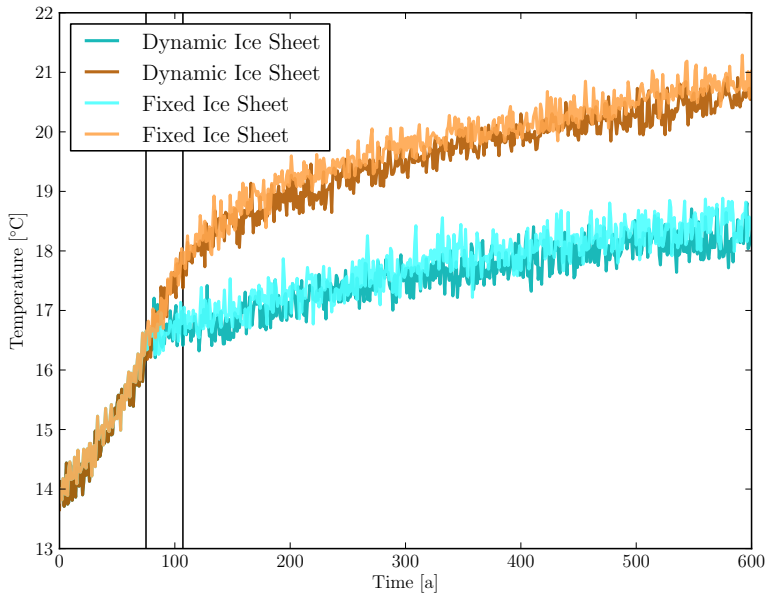

Figure 9: Timeseries of both model configurations for RCP 1% experiments. Bolder colors show the setup without dynamic ice sheets, paler colors with fixed ice sheets. As has been seen before, the introduction of the ice sheet model has a cooling effect on the global average surface temperature, which is slightly more pronouced in the higher GHG scenario.

seen in the temperature comparisons above. It is interesting to note that the albedo changes become more pronounced between the two configurations after the GHG increase has finished. This suggests that the increase in greenhouse warming is strong enough to change the albedo sufficiently quickly to overcome any differences that may be generated by the variation in model configuration, and that these changes need time to equilibrate once the system has stopped changing.

When examining the changes in albedo spatially, it appears as if the primary effect is on the sea ice, as is seen in Figure 11. Large areas in the Arctic and Southern oceans which are annually covered by sea ice in the pre-industrial control state are now ice free in the perturbed, warmer state. This reduces a large are of highly reflective ice area to a much less reflective ocean surface. A reduction in snow cover extent in the Northern hemisphere further reduces the planetary albedo, generating a positive feedback loop as the planet warms up. Differences between model configuration are minimal, with the most evident changes occurring at the high latitudes. Here, by changing the configuration to include a dynamic ice sheet, the anomaly differences are again found in those regions where semi-annual sea ice cover occurs, with primary variations attributable to the sea ice extent. There also appear to be changes in the amount of annual snow cover, particularly in the Northern Hemisphere, where even slight warming can cause a large change in the equilibrium condition dur-

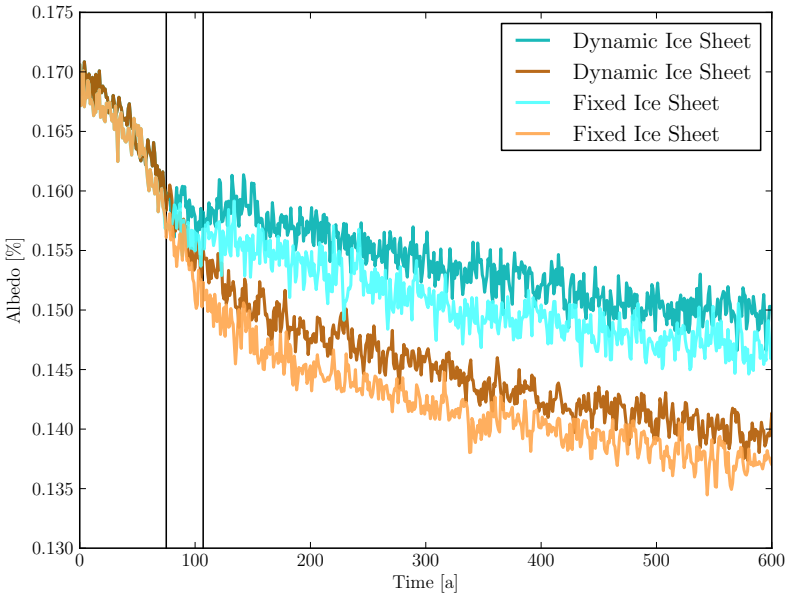

Figure 10: Time series of global average albedo. The two solid black lines mark the point at which the GHG increase has completed. A marked decreasing trend is seen while the GHG levels are increasing, with a further auxiliary reduction of albedo once the levels stabilize. The orange colors represent the forcing scenario with higher CO_2 values, the blue ones show the scenario with lower values. Bold colors show the simulation progression of the configuration with dynamic ice sheets, pale colors show the simulation with fixed ice sheets.

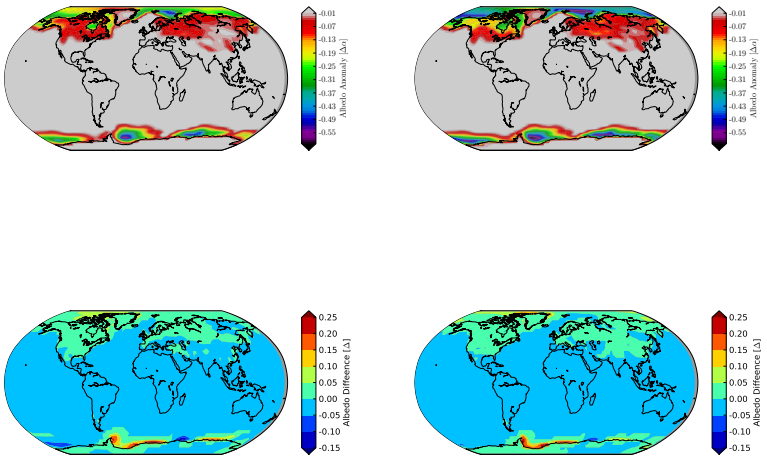

Figure 11: Albedo changes seen by the atmosphere subcomponent by the end of the experiments. The upper left panel (RCP4.5) and upper right panel (RCP6) show changes between the `aoi` setup and the control state, whereas the lower two panels show changes between `aoi` and `ao`, with positive values indicating higher albedo in the setup with dynamic ice sheets. The higher albedo values in the `aoi` setup are simulated primarily in the Northern Hemisphere, with a particularly strong signal in sea ice areas around the ice sheets, suggesting that sea ice change between the two model configurations has a strong local effect on the albedo.

ing the winter months, as large areas will no longer be below the freezing temperature.

3.1.3 Precipitation

In general, an intensification of the hydrological cycle takes place with the increase in greenhouse gas and warming. Including the ice sheet model does not necessarily have a marked effect on the spatial distribution or the global average amount of rainfall. Presented here are the spatial distribution anomalies to the control state of the experiments, the changes introduced by incorporating the ice sheet model, and time series of the absolute amount of rainfall.

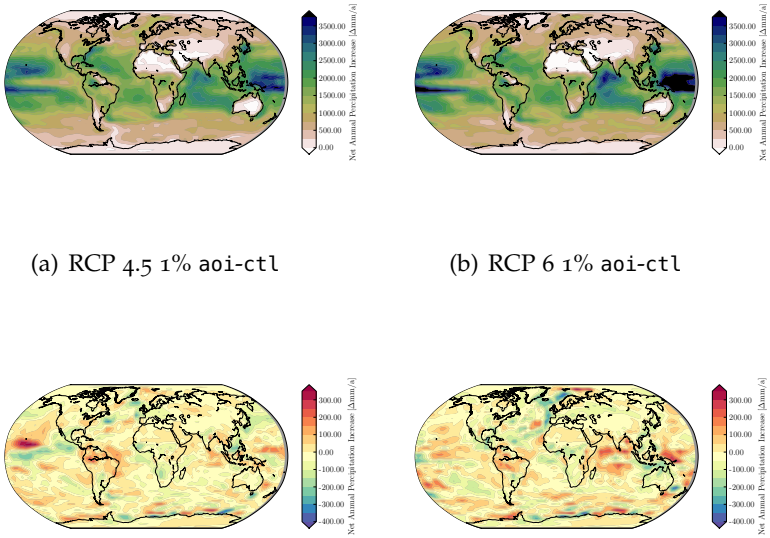

(a) RCP 4.5 1% `aoi-ctl`

(b) RCP 6 1% `aoi-ctl`

(c) RCP 4.5 1% `aoi-ao`

(d) RCP 6 1% `aoi-ao`

Figure 12: Precipitation changes seen by the atmosphere subcomponent by the end of the experiments. Panels setup is identical to Figure 11. While the configuration anomalies show a rather mixed signal globally, the lee side of the GIS gets drier in both scenarios.

Figure 12 shows that the precipitation increase is focused in the tropics and generally that the oceans will experience a larger increase than the continents. The higher latitudes do not increase as much. The differences in configuration, shown in the lower panels, show that including the ice sheet does not generate any immediately recognizable patterns or shifts in the rainfall amounts. Despite this, examining the areas around the ice sheets reveals an interesting feature, albeit a small one. The areas behind the Greenland ice sheet seem to experience a decrease in the amount of rainfall received when coupling the dynamic ice sheet model. This is seen in the green bands in the lower

to panels of Figure 12 The effect is especially pronounced in scenario RCP6 (lower right panel)

When examining the global average in Figure 13, it can be seen that the increase in rainfall parallels the increase in temperature, but since the ice sheet model does not directly affect any atmospheric variable that would lead to a noticeable difference in the amount of rainfall received, the two curves do not have any significant differences when comparing model configuration.

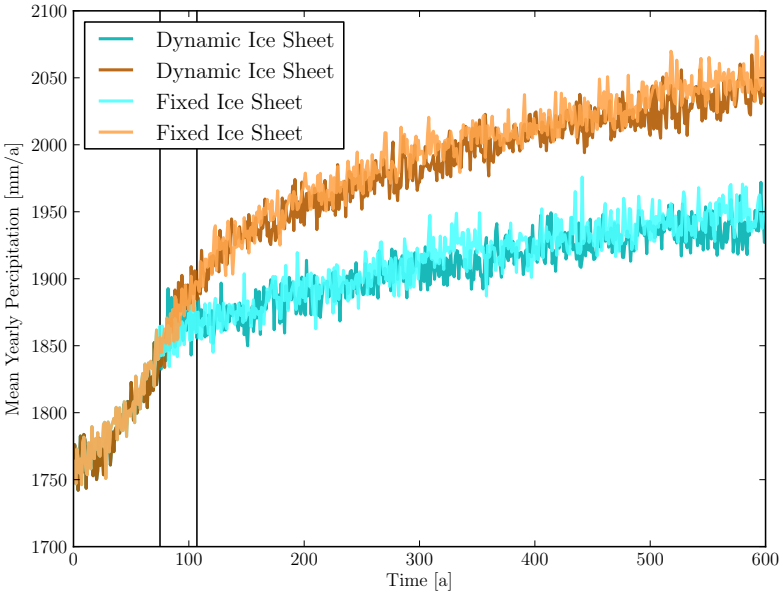

Figure 13: Time series of global average rainfall. The two solid black lines mark the point at which the GHG increase has completed.

3.2 OCEAN COMPONENT MPI-OM

While no direct forcing was applied to the ocean in terms of which inputs it was given to work with, MPI-OM undergoes changes due to its coupling with the atmosphere. Since an overall increase in global surface temperature is seen in all scenarios, changes associated with ocean warming are seen in several phenomena.

3.2.1 Changes in ocean surface temperature

The uppermost layers of the ocean, being in direct contact with the atmosphere, are the first to react to an increase in atmospheric temperature. As might be expected, the surface layers of the ocean warm up. It is no surprise that the runs forced with scenario RCP6 warm up more than those forced with scenario RCP4.5.

Before examining the spatial patterns of ocean surface warming, an overall global mean is presented. The slightly bolder colors represent

the model setup including the dynamic ice sheet, the slightly paler ones the model setup without the dynamic ice component. All runs correspond to a 1% per year increase of greenhouse gases.

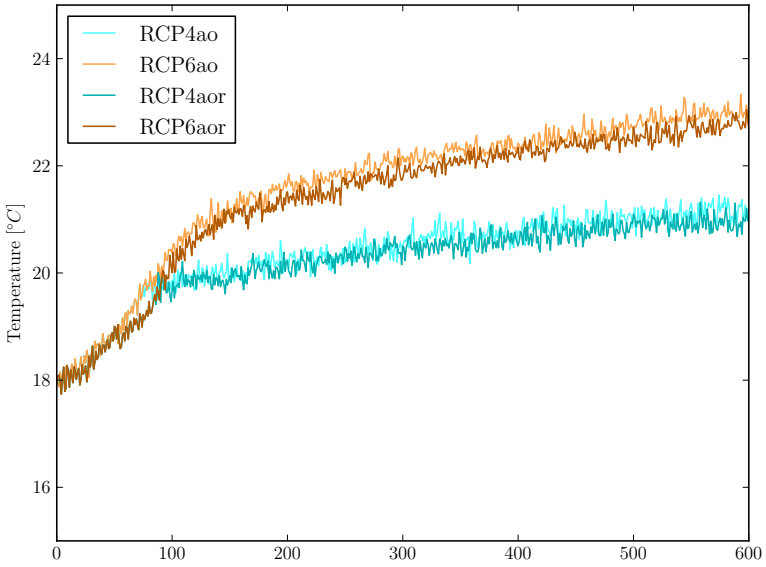

Figure 14: Time series of ocean surface temperature in RCP 4.5 and RCP 6 1% runs.

As can be seen in the figure, including the ice sheet has a slightly cooling effect on the global ocean, this is an inherited feature, as it was first seen in the atmospheric simulation. This is caused by the coupling mechanism between the two model components, as the atmospheric 2 meter temperature is directly connected the ocean's surface layer temperature. The differences between the model configurations appear to increase as the simulation progresses, although the behavior is very similar. RCP4.5 scenarios warm up by around 2.5 °C, whereas the RCP6 scenarios warm up by 4.5 °C. It should be noted that this is signal is spatially averaged over the entire ocean and temporally averaged over the entire simulated year, and that spatial differences not only exist, but are of importance for certain ocean phenomena as will be seen later on.

When examining the state at end of the simulations, it becomes possible to examine changes introduced by including the ice sheet component. Shown here are the ocean control state, anomalies to the control state for the configuration with ice sheets, and anomalies between the two model configurations for the end of the simulation. Values are 30 year climatological means.

While both configurations show a warming of the surface ocean with amplification in the polar regions, the `aoi` configuration is between 1 and 3 degrees cooler. This cooling is most pronounced in the scenario with higher CO_2, and seems to be geographically maximized in the North Atlantic. The configuration with ice sheets does not have as large of a cooling effect in the lower scenarios, suggesting

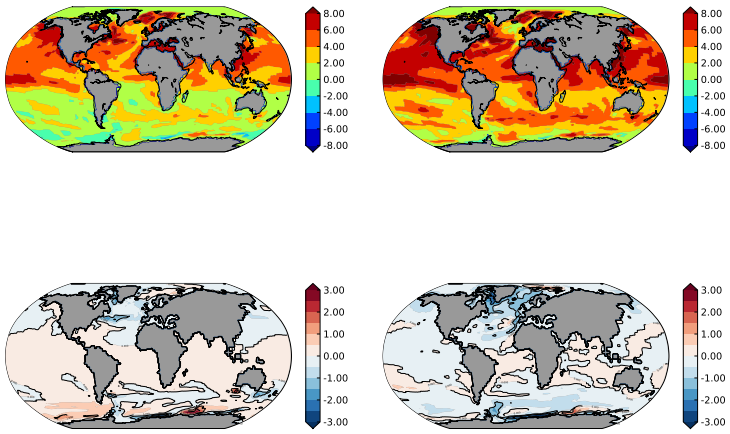

Figure 15: Differences to the control state are shown in the upper two panels, differences arising from model configuration in the bottom two. RCP4.5 is on the left, RCP6 on the right. A general cooling of the surface ocean can be seen in the North Atlantic due to the introduction of RIMBAY, which is stronger in the higher scenario. To highlight differences, contour lines of every 1 degree are shown in the bottom plots. Units are in °C.

that the ice sheet's response is temperature dependent, and that the response communicated to the atmosphere is also proportional. By including the ice sheet component, the atmosphere is modified; as the pressure changes, wind fields are shifted or weakened, and as a result sea-ice formation as well as transport of the melted sea ice and land ice are all affected. The update of ocean temperature due to sea ice melting is treated directly my the ocean model's sea ice component. The ocean-ice interface is governed by the heat balance:

$$\rho_w c_w \Delta z_1' \frac{\partial \hat{\theta}_1}{\partial t} = (1 - I) Q_w + I(Q_{cond} - h_i \rho_i L_i)$$

with

ρ_w	Density of sea water
c_w	Specific heat of sea water
$\Delta z_1'$	Depth of 1st ocean layer
$\hat{\theta}_1$	Potential temperature of 1st ocean layer
Q_w	Heat flux over water
Q_{cond}	Corrected heat flux over sea ice
h_i	Effective thermodynamic sea ice thickness
ρ_i	Density of sea ice
L_i	Latent heat of fusion of sea ice
I	Fraction of sea ice coverage

The model is restricted from increasing the temperature of the upper layer as long as there is sea ice covering it. Effects of salinity on freezing and melting temperatures are not included, as these are second order affects.

3.2.2 Salinity Changes

As the modeled earth warms up, it causes the hydrological cycle to intensify, as well as sea ice and ice caps to melt. Therefore, it is expected that the salinity of the global ocean should slightly decrease with time. Shown here is a time series of global surface layer salinity, as well as differences between the spatial patterns for both model configurations.

As seen in the Figure 16, it does not seem as if there is any significant difference based upon model configuration in terms of the global trends. The scenario with a higher ending CO_2 value has a larger salinity decrease, explainable through a higher melting amount and a more vigorous hydrological cycle.

As with temperature, it is important to ascertain where including the ice sheet will affect sea surface salinity. The figure shown below has a similar setup to Figure 15.

Figure 17 demonstrates that the primary freshening of the surface layers occurs in the northern polar regions, seen in the upper two panels. The patterns suggest that the freshening is closely tied to sea ice, as it is the same area that is seasonally covered with ice in the control state. The increase itself has a relatively large magnitude, with changes of up to 4 psu occurring in regions where strong melting occurs. Additionally, a pronounced dipole forms in Scenario RCP 6, switching between strong freshening (between -2 and -4 psu) and salinification (between +1 and +2 psu)

Examining the differences between the two configurations reveals an interesting freshening of the North Atlantic, particularly around the area of the dynamic ice sheet, which is due to runoff from the molten sheet ice. The warmer climate scenario seems to have a stronger change in salinity, although it is more localized to the North Atlantic

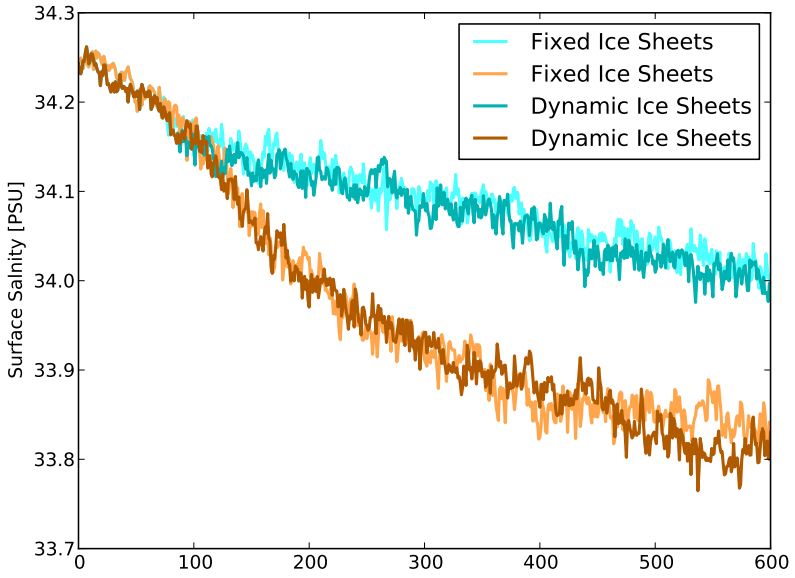

Figure 16: Timeseries of the globally averaged salinity evolution of the uppermost ocean layers. A strong decrease in the salt content is seen, which appears to be well correlated with temperature, and thereby also with freshwater input. Scenario RCP6 continues to decrease strongly, while RCP4.5 has a slight auxiliary decrease which appears to be leveling off at the end of the simulation.

Ocean. As was seen in the absolute salinity changes in the upper panels, the lower panels, showing changes between model configuration, demonstrate that including the dynamic ice sheets seems to amplify this effect further. The North Atlantic is overall fresher in the model with dynamic ice sheets, and the warmer scenario is further differentiated between North Atlantic and South Atlantic. Both absolute changes and anomaly changes between the model configurations show a pronounced dipole effect around the equator. This feature will be analyzed in detail in the next chapter, along with other changes to the freshwater and corresponding salinity budgets.

3.2.3 Features of the Control State

The following aspects of the ocean will be discussed in detail in the next chapter, since they play an important role in the freshwater balance of the North Atlantic, which in turn is connected to ability to form deep water.

3.2.3.1 *Sea Ice*

Sea ice coverage in the north Atlantic, both seasonal and inter annual, are subject to changes due to alteration of the background climate state. Of primary concern in the face of global warming is the reduction of sea ice extent, which has implications for both the Arctic albedo and oceanic freshwater balance due to brine rejection upon sea

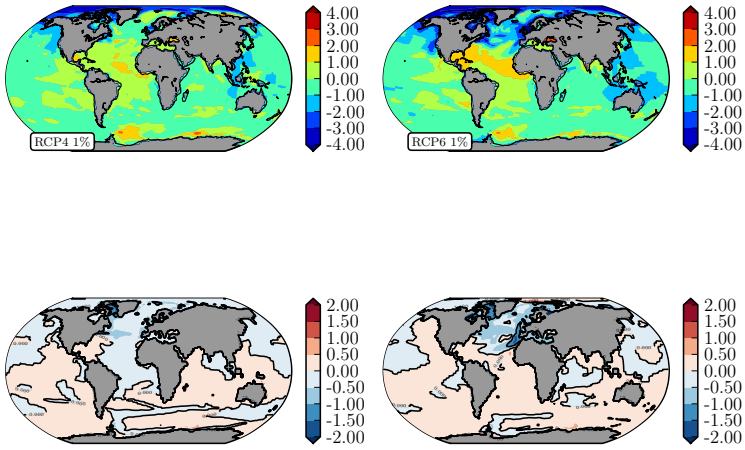

Figure 17: Changes to the surface layer salinity at the end of the simulation, with changes introduced due to model configuration. The upper panels show the difference between the atmopshere-ocean-ice setup to the default control state. A slight freshening is evident, particularly in areas around the GIS and where sea ice melting is occurring. In the stronger CO_2 scenarios, a bubble of relatively salty water is trapped in the Caribbean, which can no longer be exchanged with the North Atlantic as the downwelling has been significantly reduced. The introduction of the ice sheet has a general freshening effect on the North Atlantic in both forcing scenarios.

ice formation and freshwater injection due to sea ice melting. Shown here is the seasonal representation of the sea ice fraction.

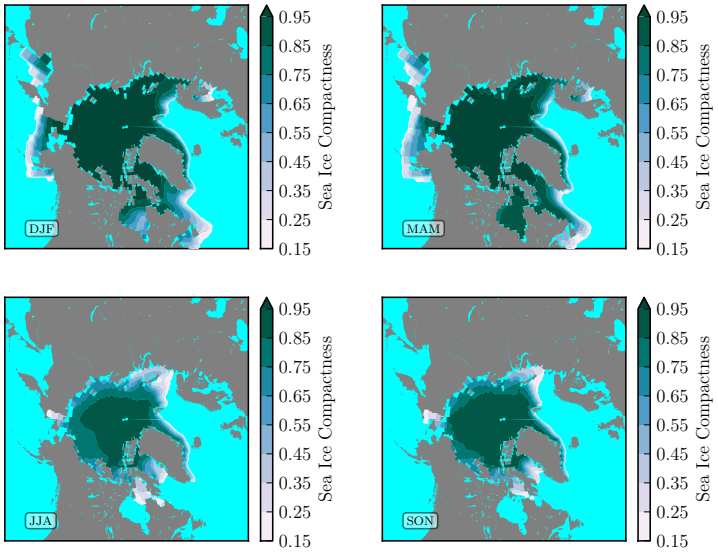

Figure 18: Seasonal sea ice coverage in the control state. Top left shows winter, top right spring, bottom left summer, and bottom right shows fall. The unit of "Sea Ice Compactness" is a measurement of how large of a fraction of the grid box is covered with ice. A distinctive sea ice retreat is seen in summer months with a limited recovery in fall, with the maximum extent reoccurring in winter.

As has been seen in satellite measurements, the sea ice fraction is maximized in the winter and spring months, with almost all of the Arctic Ocean covered with sea ice, whereas summer and fall months reduce the coverage towards the pole, exposing the Nordic Seas.

3.2.3.2 *Mixed Layer Depth*

The mixed layer depth, defined in the model as the depth at which a density difference criteria is exceeded:

$$\Sigma_1^k \delta\rho_{insitu}(z) = 0.125\,\mathrm{kg\,m^{-3}}$$

Since the model uses discrete layers of varying thickness, the mixed layer depth is the sum of all layers This is the depth where the density has increased by $0.125\,\mathrm{kg\,m^{-3}}$ as compared to the value in the surface box. [55] Shown here in Figure 19 is the spatial distribution of the mixed layer depth in the control state of the model.

Three distinct regions form with a deep mixed layer, allowing for the formation of deep water, which is a driving mechanism for deep ocean convention. As will be discussed later when freshwater balance of the North Atlantic is analyzed, the mixed layer depth is (per definition) very sensitive to changes in surface density. As a melting phenomenon will have impacts on the surface layer density, the two

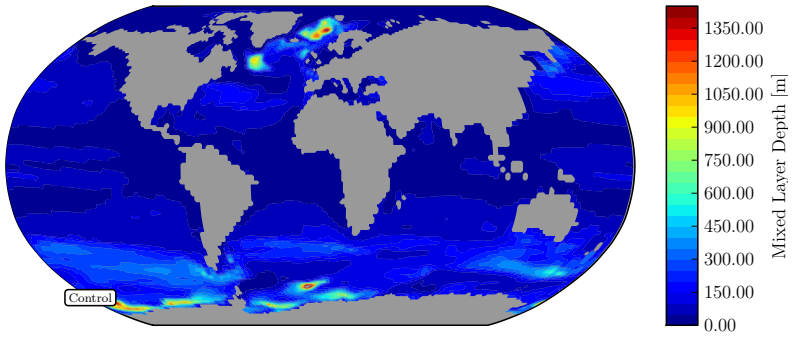

Figure 19: Mixed layer depth in meters as simulated in the control state. 3 distinct downwelling zones form, as are also seen in nature. Two form in the North Atlantic, corresponding to the Nordic and Labrador Seas, and one forms in the Antarctic.

deep convection sites in the North Atlantic will be perturbed, and this will lead to an alteration of the THC system's behavior.

3.2.3.3 *Surface and Deep Circulation*

Both surface and deep ocean circulation are import features of the climate system, as the ocean is responsible for heat transport, due to water's high heat capacity in comparison with the other components. Surface transport enables changes in salt, temperature, density as well as other physical and chemical water signals to be communicated locally to other parts of the ocean, whereas deep ocean circulation achieves this on a global scale. It should be noted that surface transport is very fast in comparison to deep circulation, which takes place on the order of a thousand years.

The surface transport is primarily wind driven, allowing the upper 100-200 meters to be circulated [42]. The depth of the wind driven component varies, but the amount of impulse generated by wind decreases with depth due to friction, giving gyre circulation a generally shallow characteristic when compared to thermohaline circulation. Shown below in Figure 20 is the control state's upper ocean layer velocity.

The deep ocean circulation is driven by changes in density, resulting from an imbalance in salt and temperature. As was seen in Figure 19, deep water formation sites exist in the North Atlantic and Southern Oceans. Shown below in Figure 21, one can see the transport of water in Sverdrups.[3]

3 1 Sverdrup = $1\,\mathrm{m}^3\,\mathrm{s}^{-1} \times 10^6$

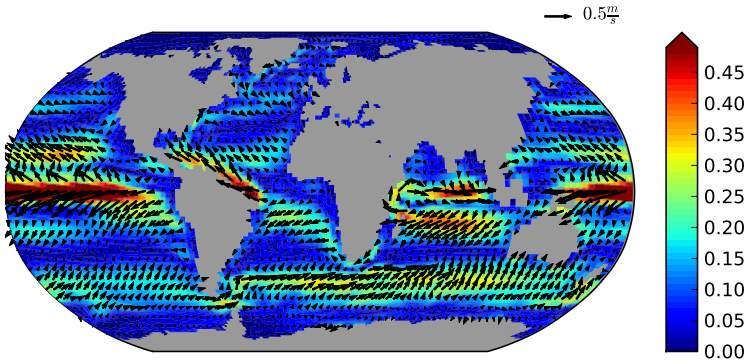

Figure 20: Surface Velocity in the Control State

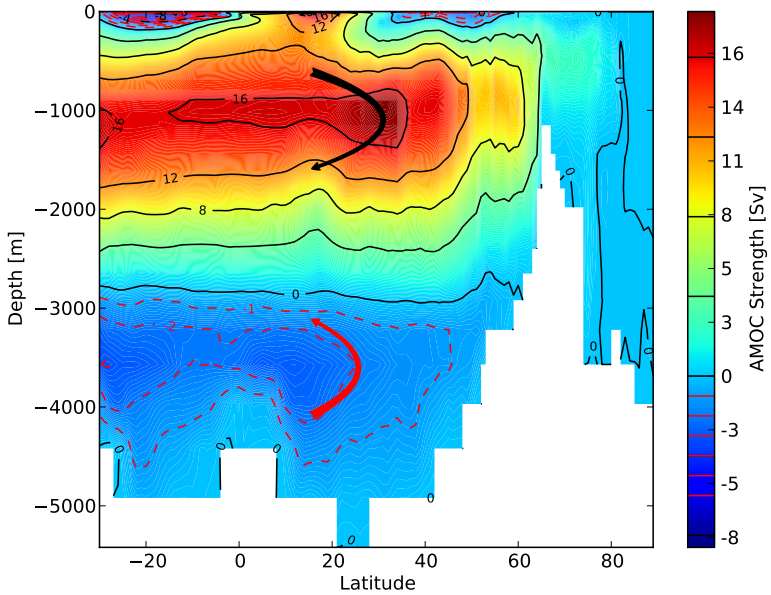

Figure 21: Streamfunction of the Atlantic Meridional Overturning Circulation in the control state. Shown is a 30 year climatological mean at a preindustrial state of 280 ppm GHG. Units are in Sv.

Positive values are defined as transport from the south to the north, and one can see 2 distinct transport features in the figure. A fairly strong northward transport develops at around 1000 meters, moving water from the equator towards the North Atlantic. The downwelled NADW is transported to an intermediate depth at the tip of this positive cell. A negative cell also develops, consisting of Antarctic Bottom Water (AABW). This transport is counterclockwise, transporting water at depth from south to north and in the upper part of the cell from north to south.

3.3 ICE SHEET COMPONENT RIMBAY

The atmospheric warming together with changes in the hydrological cycle generate conditions that force the Greenland and Antarctic Ice Sheets to alter their states. Since the focus here is on the North Atlantic, the Greenland Ice Sheet shall be examined.

3.3.1 Changes in Ice Sheet Surface Temperature

As was briefly demonstrated in Figure 5, the ice sheet model requires surface temperature and accumulation information in order to compute a mass balance. Changes in surface temperature of the ice are communicated directly from the simulated atmospheric 2m temperature.

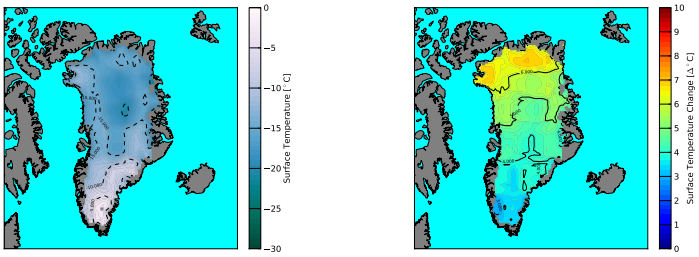

Figure 22: Surface Temperature after 600 years in the RCP4.5 1% Scenario, with anomalies to the control state.

As can be seen in Figure 22, the temperature remains well below 0 °C for a large portion of the ice sheet. Most of the warming occurs along the northern coast, although this region still remains below freezing; only the southern tip warms enough to cause the ice to melt.

While the ice sheet temperature is an important indication of where the ice will melt, knowing the overall mass balance is also crucial, therefore we also examine accumulation and ablation of the ice sheet, as well as internal dynamics that may cause the ice masses to shift.

3.3.2 Mass Balance

In general, the mass balance of an ice sheet at any given location is dependent on a combination of surface processes (runoff and precipitation) and internal ice dynamics [51]. These processes are subject to not only seasonal cycles, but also to the background climate. Shown below are accumulation, ablation, and internal ice velocity. A combination of these variables allows for an estimate of the mass balance.

3.3.2.1 *Simulated Mass Balance*

Below in Figure 23 we see the ablation and accumulation of snow on the ice sheet surface as a yearly mean value at the end of the model run for scenario RCP4.5 1%. As was seen from the temperature, a pronounced Ablation zone is seen at the southern tip of the Ice Sheet, where temperatures permit melting. Accumulation is controlled by snowfall, which is in turn regulated by elevation and convective precipitation processes. The combination of these processes describe the surface conditions an ice sheet undergoes when building up or melting away ice cover.

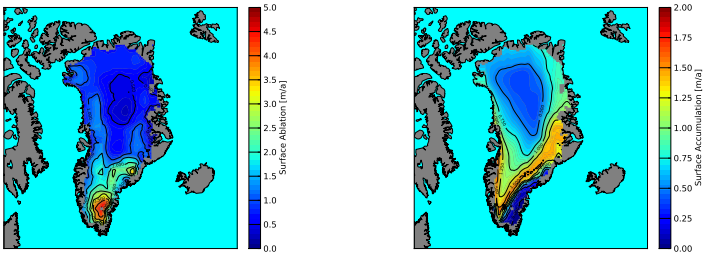

Figure 23: Greenland Ice Sheet Ablation and Accumulation in RCP4.5 1%

Internal ice dynamics allow the ice sheet, which only partially behaves plastically, to flow given certain pressure and force regimes. While factors like shear and stress are also relevant for the way in which the ice sheet can flow, the variable that should be examined is velocity.

Expressed in meters per year, Figure 24 shows that a majority of the ice is not in motion, yet at the edges where melt rates are higher, the ice flows forwards to replace the ice that is lost. While some of these velocities may seem unreasonably high, satellite radar interferometry measurements have detected speeds varying between 90 and 220 kilometers per year. [36]. Additionally, ice streams have velocities that are typically on a similar order of magnitude [14]. Recent studies have also shown that ablation zones experience velocity increases induced by melting [50].

Using a combination of these factors, it is possible to construct a total mass balance for the ice sheet and estimate how much freshwater will be exported into the North Atlantic due to melting.

The plot of mass balance reveals, as expected, a mixture of surface and internal processes. It is interesting to note a small positive mass

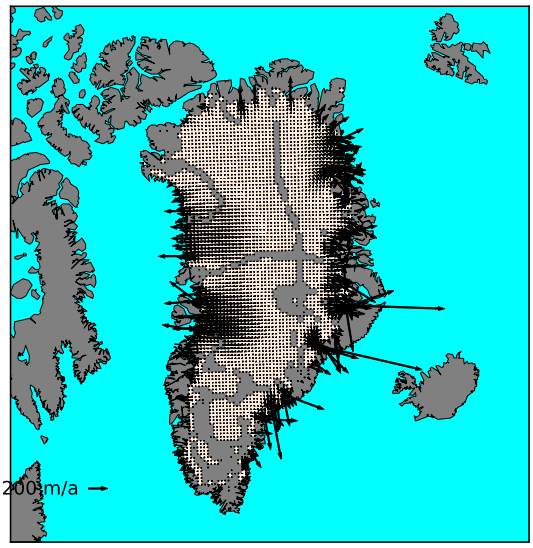

Figure 24: Mean Ice Speed, showing transport from the ice interior to the ice sheet's edge.

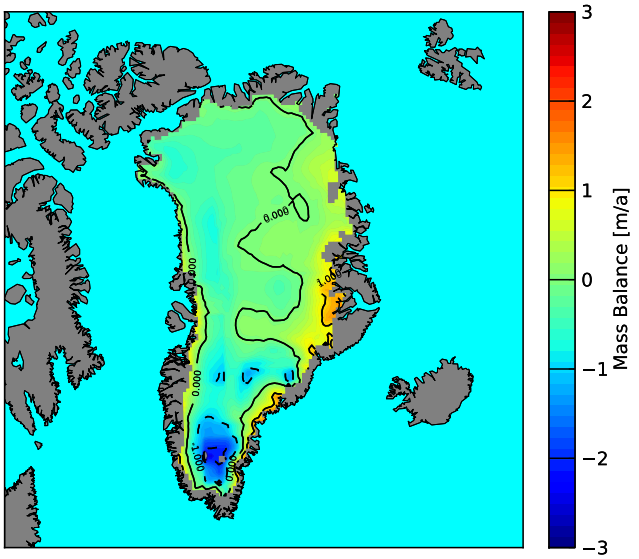

Figure 25: Complete simulated mass balance of the GIS. A pronounced zone of negative mass balance is seen in areas that are above the melting point as well as slightly smaller negative bands along the western coast

balance zone is located on the eastern side of the ice sheet, which is due to an increase in accumulation and a temperature that is below the freezing point, ensuring that precipitation falls as snow.

The figures presented here are static representations of the ice sheet at the end of the model simulation. It is of additional interest to compare these to other scenarios as well as to see the evolution of these features with time. In general, as was seen with the atmospheric results, the ice sheet reacts similarly under a climate with amplified warming as in scenario RCP6, with the exception that the patterns of melting simply have a larger magnitude.

3.3.2.2 *Comparison to Measurements and Observations*

Over the past several decades, many observations have been made of temporal evolution and increasing changes of Greenland's mass balance. Comparing the simulated mass balance results to the measured ones allows for a rough estimation of the ice sheet model's ability to generate a realistic projection. Shown below in Figure 26 is the simulated mass balance for the Greenland Ice Sheet of all 6 Scenarios and a comparison plot to measurements taken from Rignot [37].

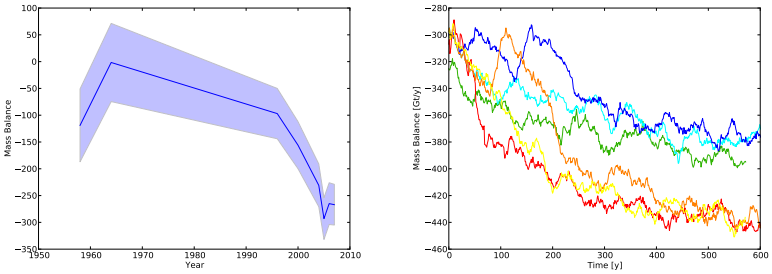

Figure 26: Simulated mass balance of the Greenland Ice Sheet for all 6 Scenarios. Despite scarce data in the Rignot observations, the simulated mass loss is very similar to observations towards the end of the century.

Further observations estimate the current mass balance of the Greenland Ice sheet to be 286 Gt/y [53], and several measurements have found this ice reduction to increasing with time. [3, 7, 52]

3.3.3 Comparison of Emission Scenarios

It is important to note that the differences between the emission scenarios, varying both in emission rate and ending concentration, seem to have only a limited effect on the ice sheet. The differences in ending ice sheet volume are presented below in Figure 27.

It becomes clear that the melting phenomena of the ice sheet do not vary significantly between emission rates, rather, the ending concentration is key in determining the characteristic shape of the ice volume evolution. This is best seen by examining the slope of the plots, which are more dependent on the ending GHG level. Indeed,

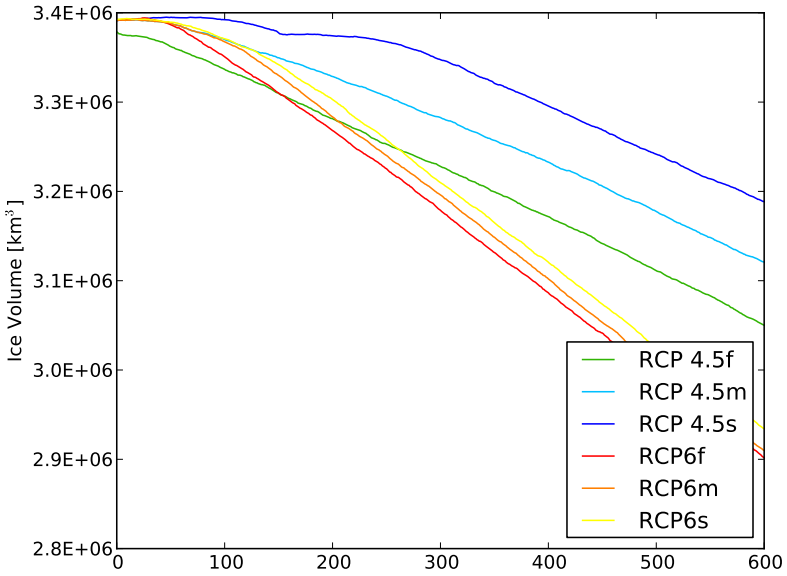

Figure 27: Evolution of the volume of the Greenland Ice Sheet

the slopes of the ice volume time series are parallel for the emission levels, and vary simply upon the timing of when the melt begins.

From the changes in ice volume, which do not show any signs of stabilizing once again, it seems that there is a definite tipping point for the greenland ice sheet. Whether this is simply a feature of the simulation or a distinct characteristic of possible future climate states is not yet clear, although some work has been done suggesting that an elimination or severe reduction of the ice sheet is possible. [8, 17, 34, 35, 38]

4 NORTH ATLANTIC FRESHWATER BUDGET

4.1 EVOLUTION OF SALT BUDGET OF THE NORTH ATLANTIC

While time series of ocean surface salinity where shown earlier in Figure 16, these were a representation of the global ocean, not the North Atlantic specifically. The specific region selected for the analysis is shown in Figure 28

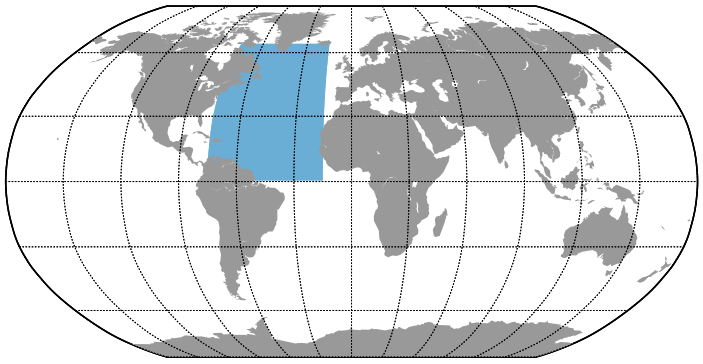

Figure 28: Region selected for freshwater budget analysis

Shown here are evolutions of surface, mixed layer, and deeper salt content within the North Atlantic Basin. The differences are most pronounced at the surface layer, with changes to the model configurations demonstrating a freshening of about 1 psu. Interestingly enough, the weaker CO_2 scenario shows a recovery towards the control state, while still maintaining a separation due to model configuration. The stronger scenario demonstrates a consistent freshening as time progresses. The freshening in the RCP_4 scenarios can be attributed to land ice melting, which explains why the model with dynamic ice sheets remains fresher. Since other sources of freshwater (sea ice and rain) do not change as much with the smaller amount of warming, the surface layer is eventually able to recover.

This is not the case in the deeper layers. Just below the mixed layer, the salt content increases. As will be seen later on, this is a result of changes to the deep ocean circulation. As formation and transport

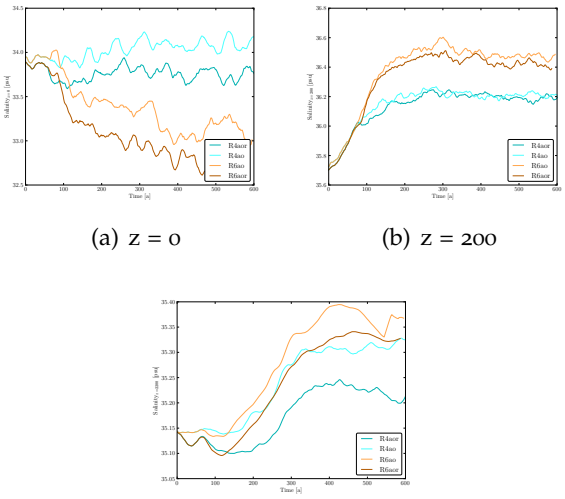

(a) z = 0 (b) z = 200

(c) z = 2200

Figure 29: North Atlantic Salinity at various depths

of deep water decreases, the transport and exchange of water masses also occurs less frequently, leading to a new equilibrium level of salinity just below the mixed layer. While the change is minimal (on the order of 0.25-0.50 psu), it suggests that changing the salinity budget in the surface layer has an impact on the lower ones as well. To better demonstrate this, a spatial plot over the entire Atlantic (regional mean of Figure 28) is shown next, with a profile of the control state along with changes to this control state in the configuration with ice sheets, and anomalies between the two model configurations.

The freshening of the surface layers can be clearly seen, as well as a slight salinification of the deeper ocean. As was seen in the time series, this is connected to a reduction of deep water formation. While the deep layers become saltier in both model configurations, the upper layer salinification at around 1500 meters is a feature that is damped by the inclusion of dynamic ice sheets, as the overall freshening of the entire water column is also communicated to deeper ocean layers. The blue bands in the anomaly plots (the lower two right hand panels), show that the salt content increase in comparison to the control state is even more pronounced in the ao setup than in the aoi setup. This suggests that there is a intermediate depth region in the North Atlantic that undergoes salinification due to changes in the surface regions, but the overall greater amount of freshening partially suppresses this in the aoi setup, generating a less intense salt increase. This is likely tied to the inability of deep water masses to mix as effectively, due to a reduction of the THC system.

These plots, shown in Figure 30, were for the entire North Atlantic. However, since the region of interest is primarily the areas of deep water formation, which will be discussed in detail in the next chapter, an anomaly plot of the top layer is shown to demonstrate where freshening is strongest.

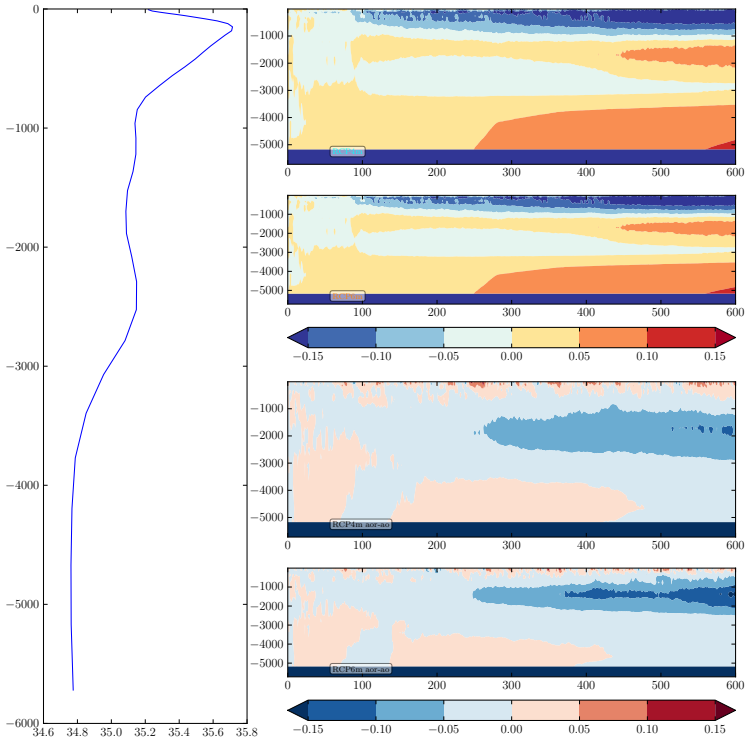

Figure 30: Salinity changes in the North Atlantic Ocean (region shown in Fig. 28) with depth over the entire simulation, units are in psu. Shown in the left panel is the control state profile, with a pronounced halocline in the upper hundred meters. The right panels show the change to this control profile at each depth level with time. In both the low and high CO_2 scenarios, a freshening occurs in the upper layers, shown in the blue lens that forms here. The lower two panels show the differences between the simulation with fixed and dynamic ice sheets. (`aoi-ao`)

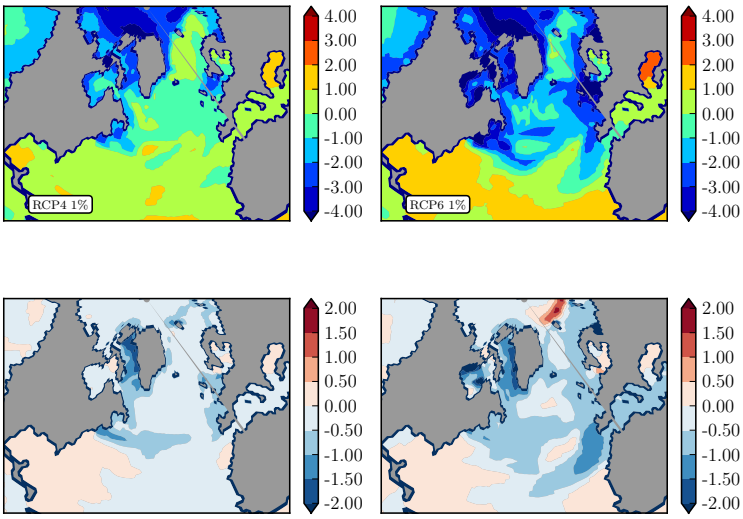

Figure 31: Changes in surface salinity as compared to the control state (upper panel: `aoi-ctl`), changes between model configuration (lower panel: `aoi-ao`). All units are in psu.

Anomalies of the dynamic ice sheet configuration to the control state (upper panel) show a pronounced freshening in the higher latitudes of the North Atlantic, while the tropics remain close to the initial salinity. Including an ice sheet increases the freshening, as expected. Interestingly enough, an increase in surface salinity is seen in the RCP6 scenario runs, extending from the Caribbean to the North African coast. As was the case with the middle and deep ocean salinification, this is connected to a weaker deep ocean circulation. Since saltier water packages can no longer be downwelled as efficiently, some of the saltier water that leaks out of the Mediterranean Sea and water that becomes saltier due to the high evaporation along the equatorial latitudes becomes trapped in the middle of the Atlantic Basin.

4.2 LAND ICE MELTING

After showing the changed salinity states of the North Atlantic, the question of where and why these changes occur arises. The largest impact on the salinity budget of the North Atlantic is due to the melting of the Greenland Ice Sheet.

The coupling scheme used to connect the ice sheet model to the earth system model preserves freshwater in the form of snow melt and ice moving across the sheet boundary. These two variables are defined to be calved and are given to the ocean via the coupling developed by Barbi et al. [2]. A time series of calved ice moving across the ice edge is presented in Figure 32

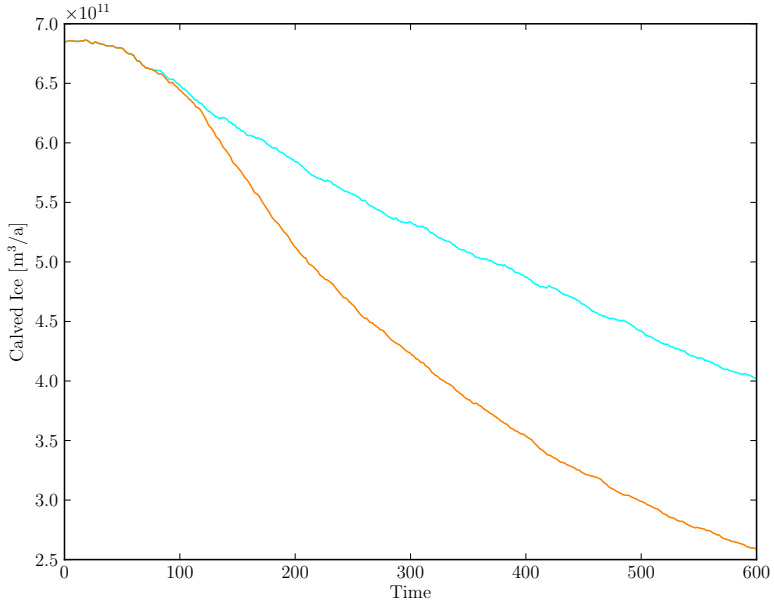

Figure 32: Calved Ice from the Greenland Ice Sheet. The blue line represents RCP 4.5 and the orange line represents RCP 6. The negative trend is caused by the way in which the model treats calving, which is defined as ice moving across the grounding line. As the grounding line is fixed in this implementation of RIMBAY, the overall amount of ice seen to be calving decreases as the ice coverage retreats.

As was also seen in the salinity values presented in Figure 31, the scenario with higher CO_2, shown in orange, seems to output more freshwater into the ocean. The reason for the negative trends in the calved ice has to do with the fashion in which the model treats it's boundaries. There is no numerical modification of the ice sheet edge as the ice sheet decreases its extent; therefore the "real" boundaries are represented inaccurately further into the simulation. As was seen in Figure 25, this especially has an impact on the southern edge of the ice sheet, where some areas melt entirely. For this region, calving that would be happening at the "new" edge is neglected, since it is still defined to be within the ice sheet's interior.

The second component of the freshwater balance is the runoff of melting snow. The ice sheet model computes this as ablation, of which a spatial pattern was shown above in Figure 23. A timeseries of the field sum of ablation is shown here, showing a cumulative amount of all ice sheet melting.

A strong seasonal and yearly variability can be seen in the simulation. The order of magnitude, however, is much lower than the amount of calved ice, as seen in Figure 32. Since ablation and calving are the only simulated mechanisms for removing mass from the ice sheet, and since all removed mass is defined in the model as freshwater input to the ocean, we can examine the complete amount of freshwater input generated by the land ice.

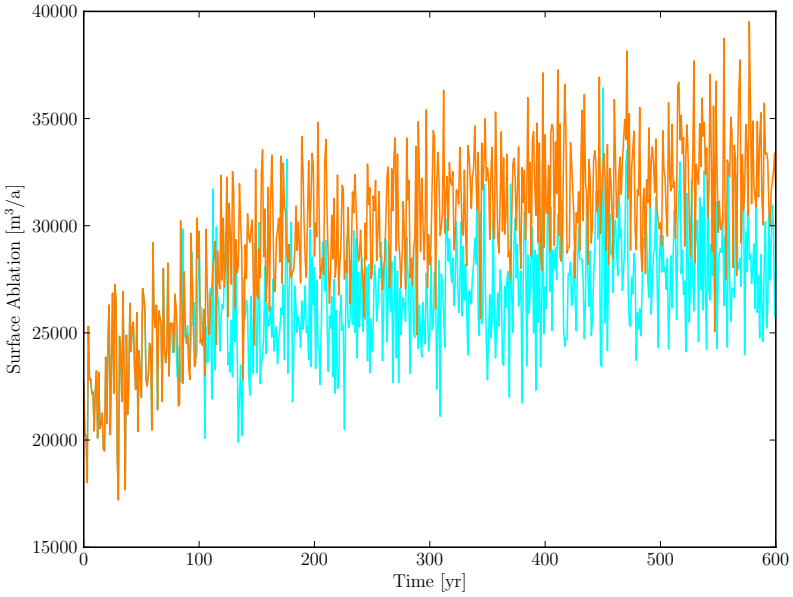

Figure 33: Timeseries of Ablation from the Greenland Ice Sheet. Both forcing scenarios show an increased ablation rate, corresponding to a warming and subsequent melting of the ice sheet. The effect is enhanced in the scenario with increased warming.

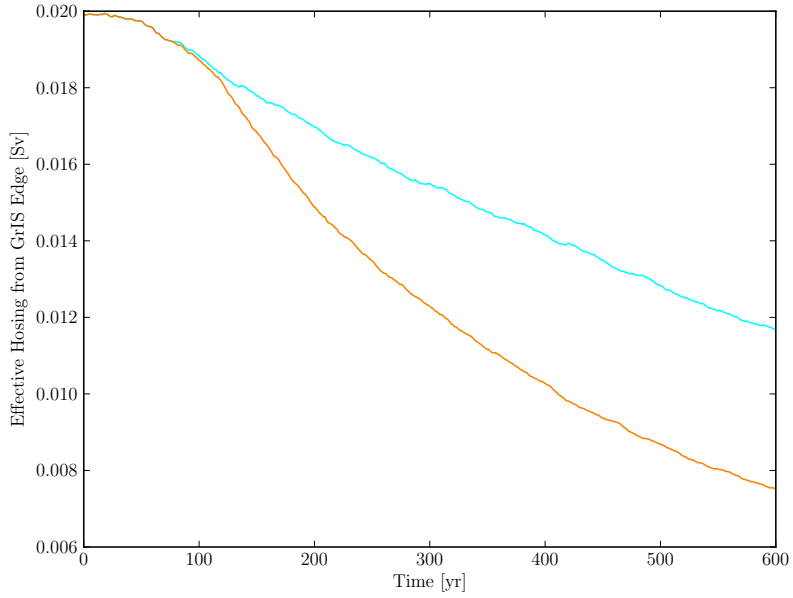

Figure 34: A sum of all possible meltwater sources from the Greenland ice sheet is presented. Due to a technical limitation at the time, calving is strictly defined as ice moving across the grounding line, which is fixed at the beginning of the simulation. As this is no longer the boundary later on, due to ice retreat, the amount of freshwater from the ice sheet is generally underestimated, explaining the downward trend.

Since calved ice has such a higher order of magnitude compared to ablation, the sum of the two terms clearly is dominated by calving. The units of Figure 34 are in Sv, which is typical for freshwater sensitivity experiments.

While processes controlling the mass balance of ice sheets, and therefore also the melting phenomena, were discussed earlier, the actual amount of ice remaining at the end of the simulation has not yet been shown. As was seen in Figure 27, the Greenland ice sheet loses between 300,000 and 600,000 cubic kilometers of ice. Shown below are representations of the percent of ice sheet thickness remaining as compared to the initial state.

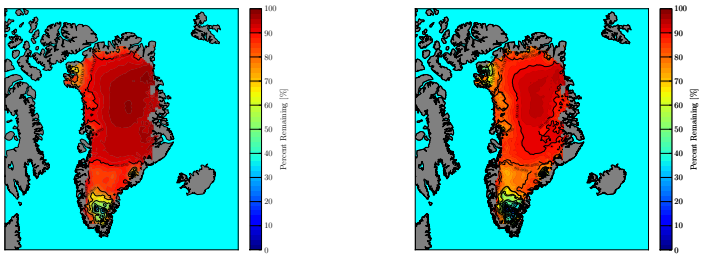

Figure 35: Percent of initial ice thickness remaining at the end of the simulations.

Regardless of ending greenhouse gas level, it appears that the response of the ice sheet is similar, shown in Figure 35. The majority of the melting takes place along the western and southern coasts, while the eastern side remains comparably stable. In particular the southern and northwestern tip melt considerably, with ice volumes reaching 0% of the initial state along the southern edge and under 50% at the northwestern tip. The remainder of the ice sheet does not undergo such severe melting.

This melting accounts for the differences seen in model configuration, leading to stronger freshening on the North Atlantic, further weakening of North Atlantic Deep Water formation, and causing the associated changes in deep ocean circulation.

4.3 SEA ICE MELTING

A second large source of salinity anomalies arising due to global warming is the melting of sea ice. Strictly speaking, the physical processes by which sea ice form do not allow for the water/brine mixture to freeze in such a way that all the salt is returned to the ocean, and sea ice contains small pockets of brine. Multi-year Arctic ice contains salt pockets comprising about 3 psu, however thinner ice may contain much larger amounts of salt.

For this reason, MPIOM is programmed to use an intermediate value of 5 psu when simulating melting phenomena in sea ice. In this sense, sea ice is not truly a source of freshwater, rather it is a source of less salty water. It does, however, allow for redistribution of salt

within the Arctic and Southern Oceans. Additionally, brine rejection can have impacts on the local salinity budget in areas where sea ice initially forms.

In order to examine the changes in surface salinity due to sea ice, several fields are shown. To begin, changes in the spatial distribution of sea ice are shown at the end of the simulation period, presented as 30 year climatological means.

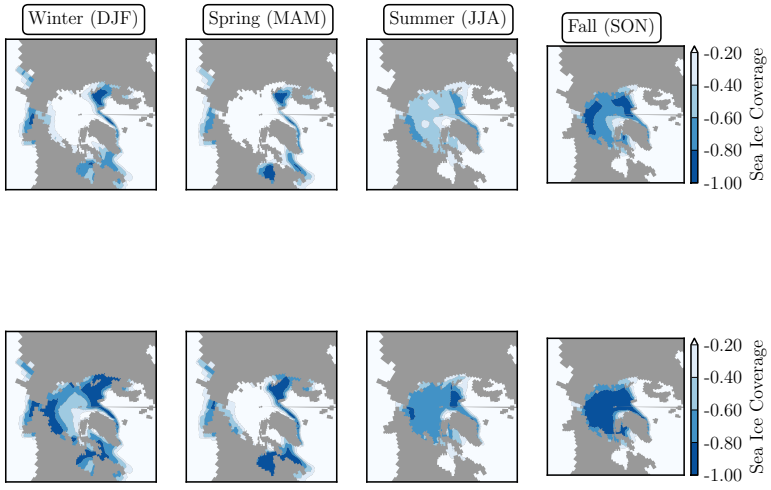

Figure 36: Changes in seasonal sea ice cover. From left to right: Winter, Spring, Summer, Fall. The Upper panel shows changes to the control state for RCP4, the lower one for RCP6. Units are fractional, such that -1.0 shows a 100% loss of sea ice compared to the control state. Fields are are 30 year seasonal means, designed to remove any multi-annual variability.

Figure 36 shows the percent of sea ice loss at the end of the simulation period as a seasonal average for the dynamic ice sheet configuration. The most dramatic loss of sea ice coverages occurs in the warmer seasons, summer and fall. Unlike other variables examined thus far, sea ice is much more sensitive to changes in temperature, since the warmer RCP6 scenario simulates a much higher reduction of sea ice coverage, even in the winter months. This has dramatic effects on the planetary heat budget, since annual sea ice coverage is responsible for a higher planetary albedo, particularly in the polar regions.

Removing the sea ice coverage almost entirely in fall and severely reducing it in winter allows the surface ocean to heat up. Furthermore, as less and less new sea ice forms each year, the amount of brine rejection that occurs reduces, altering the seasonal input of salt in winter, which occurs upon sea ice formation, and freshwater in summer, which occurs when the sea ice melts again.

To examine when exactly the reduction of sea ice cover is strongest, time series of ice area for the Arctic, North Atlantic, Greenland and Labrador Seas is shown in 37.

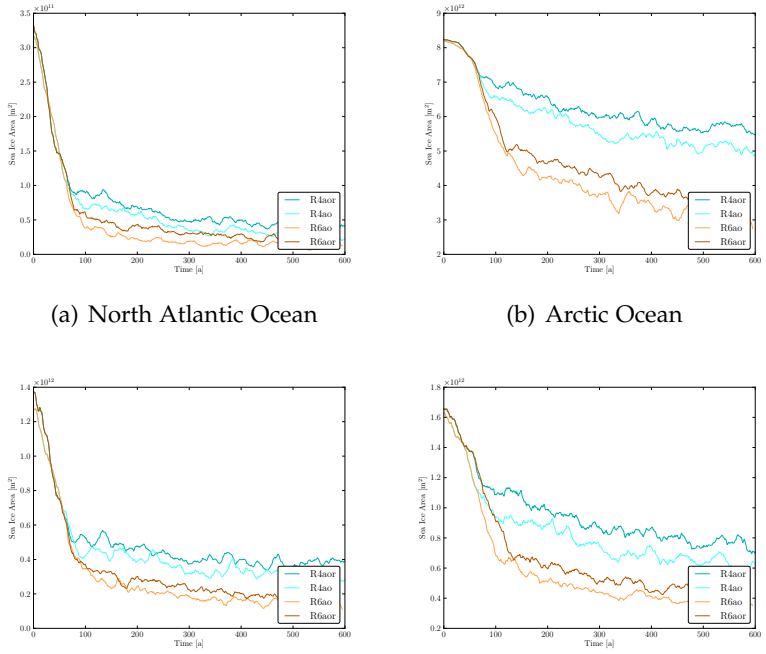

(a) North Atlantic Ocean

(b) Arctic Ocean

(c) Greenland Sea

(d) Labrador Sea

Figure 37: Evolution of Sea Ice Coverage in North Atlantic, Arctic, and Nordic Seas

As is clear from the figure, the sea ice coverage reduces strongly during the period of greenhouse gas emission, and slowly continues to adjust itself after GHG levels stabilize. The North Atlantic, being the southernmost region examined, is particularly sensitive, since little sea ice forms here to begin with. The Nordic Seas are slightly more stable, although both the Greenland Sea as well as the Labrador Sea, which is critical to deep water formation, experience severe reductions of sea ice coverage.

The timing of the sea ice cover reduction plays a critical role in how the deep ocean circulation reacts, as will be seen in the next chapter. A combination of the brine rejection and newly available heat exchange interface has impacts on the surface layer's density, which in turn regulates how easily a new deep water package can be formed.

4.4 CUMULATIVE EFFECT

Taking the effects of increased rain (shown in the previous chapter), land ice and sea ice melt into account allows for the construction of a net freshwater balance into the surface layer of the Atlantic Ocean. While the only patterns that are spatially highlighted are those from the melting of the ice sheet, the other effects are also present and can be more easily recognized in a time series of net freshwater flux over the entire Atlantic basin.

Shown in Figure 38 are the freshwater input timeseries (upper panel) for meltwater around the ice sheet, and anomalies between

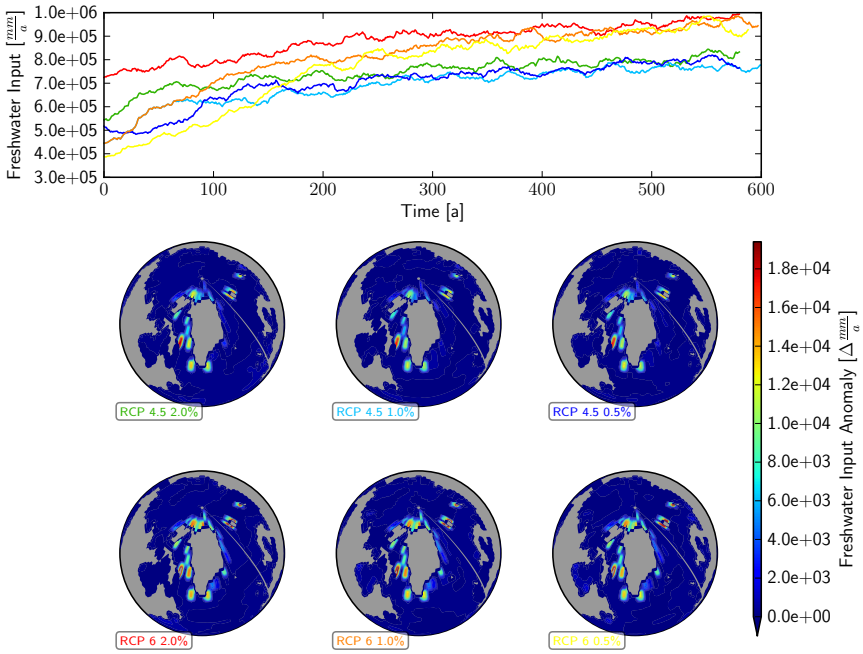

Figure 38: Spatial and temporal evolution of freshwater flux in the North Atlantic in the model configuration with dynamic ice sheets (upper panel), as well as increased freshwater input due to including a dynamic ice sheet (lower panel).

the configurations (lower panel). Timeseries of freshwater input appear to be smoothed due to a 20 year running mean that was applied. This was necessary in order to be able to distinguish the responses of each simulation, which otherwise overlap quite heavily. The rough pattern seen around the GIS is a result from the upscaling procedure required to re-interpolate freshwater input from the finer grid size used in the RIMBAY model to the coarser one used in COSMOS. To examine differences between model configuration, freshwater input as seen by the ocean can be viewed as a time series. This time, only the 1% GHG scenarios are shown.

While these signals seem to have a strong multidecadal variablilty, there is a clear distinction between both the stronger and weaker GHG forcings, as well as a clear strengthening of the freshwater input for the configuration with dynamic ice sheets. In order to gain an insight into how much extra freshwater is being pumped into the north atlantic, anomalies between the two configurations are shown as well. The p values, shown in the lower panel of Figure 39, demonstrate that there is a strong, statistically significant difference between the two models, suggesting that including a dynamic ice sheet has a significant effect on the freshwater input of the North Atlantic.

Breaking down the signal seasonally reveals that the majority of the melting occurs, as expected, in the summer months. Shown as an example in Figure 42, the freshwater flux in Scenario RCP4m varies between no freshwater input or net evaporation (ie nothing less than 0), and 30 mSv. The sum of these fields explains the time series trends seen in Figure 39. Including the dynamic ice sheet has a large effect

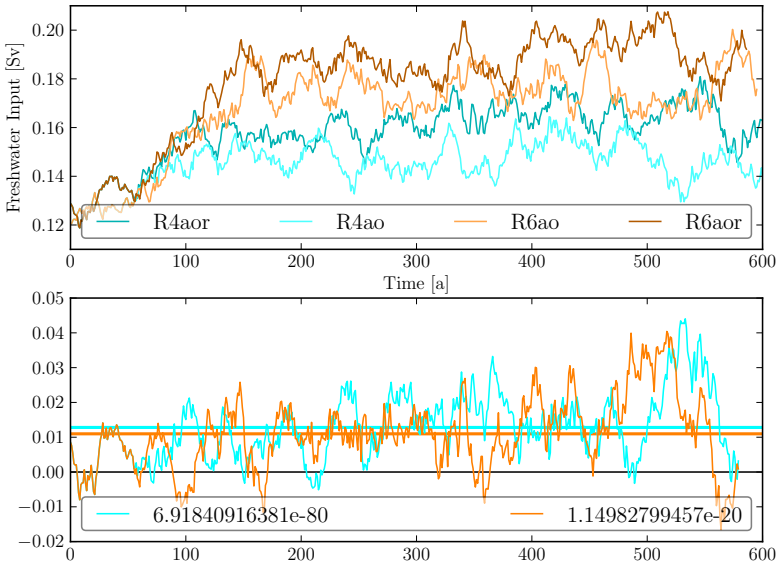

Figure 39: Freshwater Input into the North Atlantic Basin. An increase flux of about 0.2 Sv in the RCP 6 scenarios and approximately 0.15 Sv in the RCP 4.5 scenarios is injected into the upper layers of the North Atlantic. Including the dynamic ice sheet component increases the injection significantly.

on the net amount of freshwater put into the surface ocean, increasing the input by up to 10%. A slight retention of freshwater is seen in the winter months, likely due to either a shift in the amount of precipitation over the ice sheet or due to a temporal retention as snow and ice are trapped in the ice sheet before returning to the ocean later as meltwater.

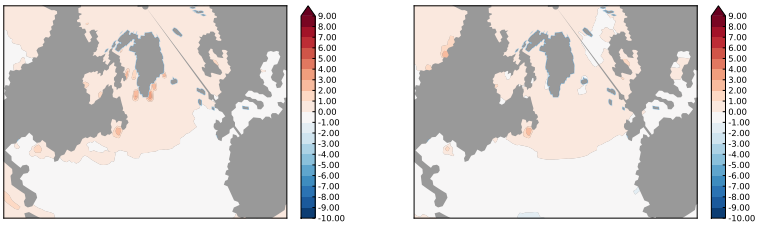

(a) Absolute freshwater flux: boreal summer

(b) Absolute freshwater flux: boreal winter

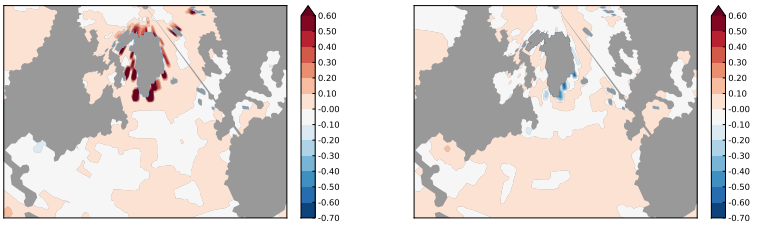

(c) Relative freshwater flux boreal summer with ISM

(d) Relative freshwater flux winter with ISM

Figure 40: Net Freshwater Flux into Atlantic Ocean, units in mSv. The amount of freshwater injected by the ice sheet is clearly seen in part (c), which amplifies the absolute amount of freshwater shown in (a). A slight retention in form of freezing ice is seen in (d), as precipitation does not immediately run off into the ocean if conditions allow it to freeze and add to the ice sheet's volume.

5 DISCUSSION

5.1 CHANGES TO THE ATLANTIC MERIDIONAL OVERTURNING

As was mentioned in the introduction, the AMOC is one primary transport mechanism for heat in the climate system. Due to the high heat capacity of water, the surface layers of the ocean are able to transport heat towards the poles, regulating the climate and corresponding weather systems in Europe and North America.

Figure 21 showed the control state of the AMOC, with a strong convective cell forming in the upper 2000 meters. The positive values indicated a clockwise rotation of the water masses, transporting surface water towards the north and returning intermediate water towards the south. Taking the core of this strong positive cell as an indicator value, it is possible to see how the overall strength of the circulation changes due to freshwater input.

Due to an increase in temperature and an increase in freshwater input, it will become more difficult to form deep water packages in the North Atlantic, since both a steep salinity and temperature gradient will form, and therefore also a strong density change must be overcome before water can sink. When this does occur, surface water flows back to replace the downwelled water according to the laws of continuity. As was seen in Chapters 3 and 4, there is a net freshening of the North Atlantic due to a variety of factors, including land and sea ice melting as well as an increase in net precipitation.

Shown here is a weakening of the AMOC in response to freshwater perturbations in the North Atlantic. The simulations with dynamic ice sheets reduce by 1 to 2 Sv more than the simulations with fixed ice sheets. It is also interesting to note that the speed of greenhouse gas emission plays an important role in the timing of the strength reduction, suggesting that temperature is a triggering mechanism for AMOC reduction, which is then further supported by increase in freshwater supply. Additionally, as the ocean re-equilibrates, the scenarios with a smaller amount of warming are eventually able to recover to a circulation strength that is similar to the control state, albeit slightly weakened. This is because the amount of freshwater and amount of ocean warming are slightly smaller than in the RCP6 case, suggesting that the AMOC is sensitive to even small changes in temperature and ocean salinity.

The simulation of an overall weaker AMOC due to the inclusion of dynamic ice sheets suggests that the future response of the system is indeed dependent on melting of land ice as well as overall warming. To better illustrate this, a plot of the overturning strength with depth

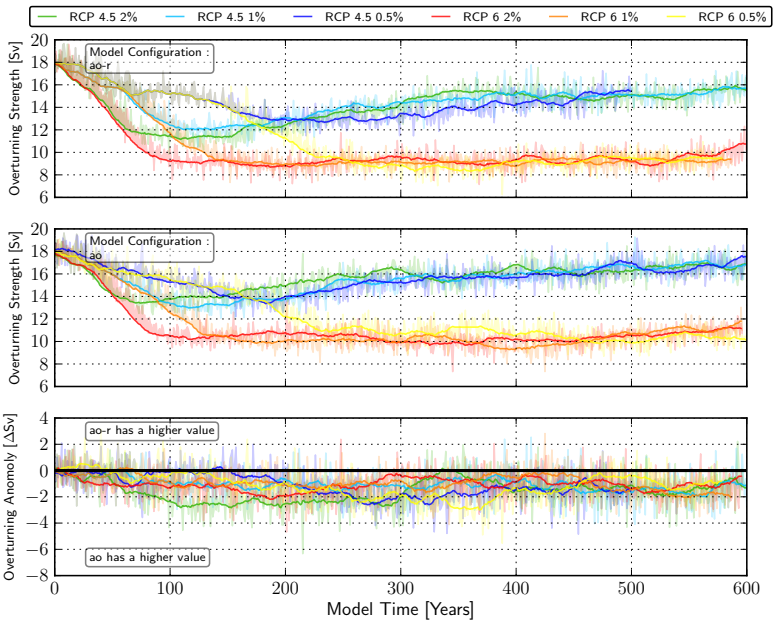

Figure 41: Changes in the maximum strength (in Sv) of the Atlantic Meridional Overturning Circulation

is presented for the scenarios with 1% GHG increase per year, along with a plot of the the control overturning state.

The overall reduction of the AMOC is immediately clear; the upper cell spanning 800 to 2000 meters weakens and retracts towards the equator. The weakening implies several changes to the internal ocean, particularly that water transport from the equator towards the polar region (upper branch of the positive cell) is reduced, and as such, less warm water is pumped towards the polar latitudes. This partially counteracts the overall warming seen due to the increase in greenhouse gases, although it is not a large enough effect to entirely compensate the warming.

Despite the overall weakening, the overall structure of the circulation remains similar. The maximum northward motion still occurs in the upper part of the ocean, and newly formed North Atlantic Deep Water is still transported south at an intermediate depth of approximately 2500 to 3000 meters. One interesting difference is the severe reduction of Antarctic Bottom Water, which is seen as a weak negative cell in lowest layers of the control state.

5.2 OCEAN DENSITY CHANGES DUE TO MELTING PHENOMENA

The mechanism for overturning is driven primarily by density gradient changes, and according to continuity, surface water flows to replace water masses that sink in deep water formation processes. As such, the density structure of those sites of the ocean where the mixed

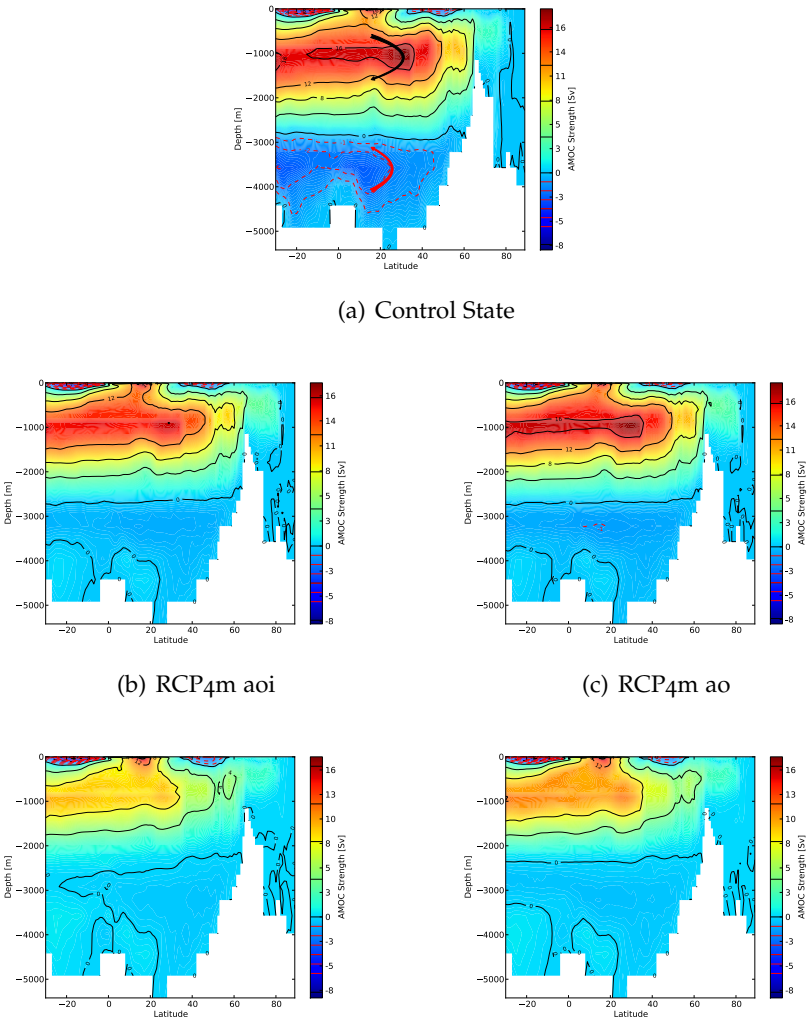

(a) Control State

(b) RCP4m aoi

(c) RCP4m ao

(d) RCP6m aoi

(e) RCP6m ao

Figure 42: Atlantic Meridional Overturning Circulation Streamfunction at the end of the simulation period as a 30 year climatological mean. Units are in Sv. A weakening of the upper positive cell is seen in all scenarios, but the RCP4.5 scenarios are able to recover to a state that is similar to the control period, albeit slightly weakened. In the case for RCP 6, the upper cell weakens significantly, and retracts towards the equator.

layer is maximized should give some insight into where and when the deep water that drives the Thermohaline Circulation is being formed.

The location of downwelling sites was shown in Figure 19; however, since these locations shift their locations with time, a slightly broader region was selected to analyze the temperature, salinity, and corresponding density changes of deep convection zones.

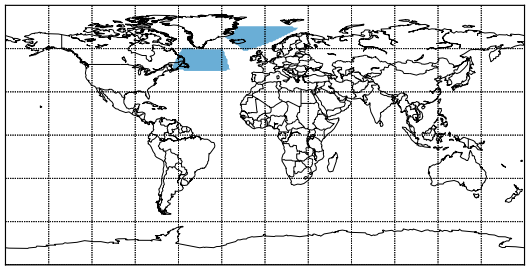

Figure 43: Region of Analysis for Downwelling Sites

The highlighted regions encompass both the Labrador Sea (LAB), and the Greenland, Iceland, and Norwegian Seas (GIN).

5.2.1 Temperature Response

Shown here are temperature responses for RCP4.5 and RCP6 1% per year increase compared to the control state. While a general surface warming can be seen in all simulation runs, the RCP6 scenario warms up considerably more than the RCP4.5 scenario. Adding dynamic ice sheets has a slight cooling effect, with decreases of the warming by approximately 0.45 degrees. As the sea ice cover melts, the ocean has the ability to take up more heat, leading to additional warming. Since sea ice cover decreases more in the setup with dynamic ice sheets, the warming here is amplified towards the end of the simulation.

Examining the GIN seas first, a warming of up to 3 degrees can be seen in the surface layers at the end of the simulations; this temperature increase becomes less pronounced deeper in the ocean. As was seen in the atmospheric responses earlier, the higher GHG scenario shows a similar pattern, although the amplitudes are increased.

The Labrador Sea, a second primary downwelling zone, also warms up considerably during the course of the simulation. Just as with the GIN Seas, the upper layers warm up more than the lower layers, and the higher forcing scenario demonstrates a similar pattern with a stronger amplitude. The differences between the model configurations are less pronounced than in the GIN seas.

Temperature is one of the two parameters that play a critical role in ocean water density; the overall warming will result in a decrease in

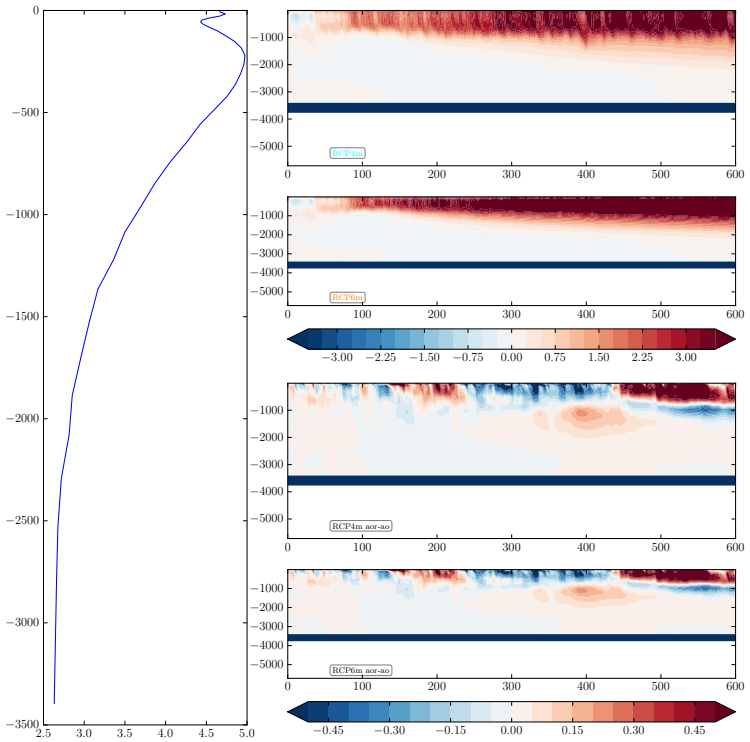

Figure 44: Warming of the downwelling region in the GIN seas, shown in Fig 43. Seen here is a large warming of 3 °C in the upper two panels, showing anomalies to the control state (`aoi-ctl`) The lower two panels show the temperature change generated by including a dynamic ice sheet (`aoi-ao`). Overall, the surface ocean is slightly cooler, although the cooling effect is not consistent throughout the water column and changes with time.

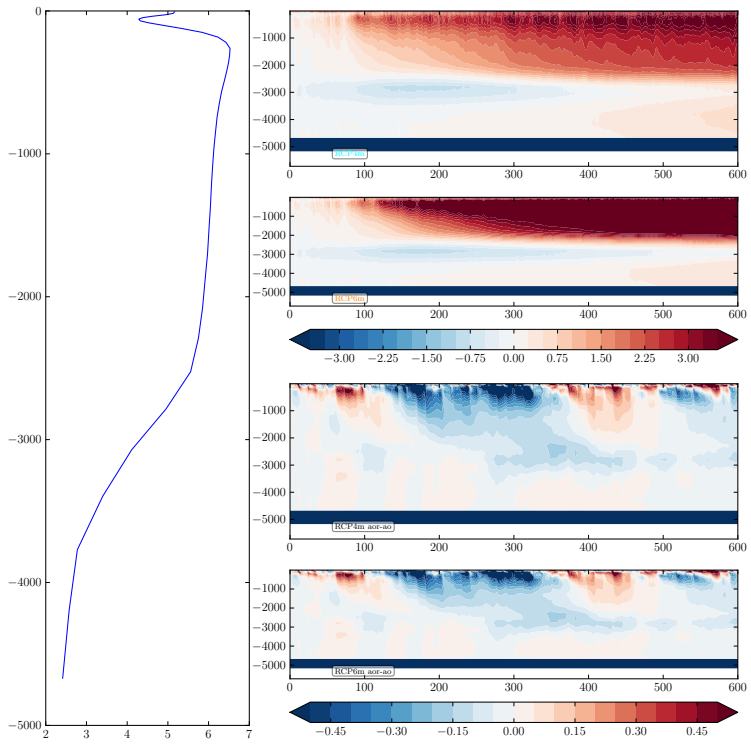

Figure 45: Warming of the downwelling region in the LAB seas. In contrast to the GIN, the warming is much stronger in this region. The anomaly between the model configurations, shown in the lower panels, shows that the `aoi` configuration simulates ocean temperatures that are 0.5 °C colder than the `ao` version.

density, making the surface layers more buoyant than in the control state. However, it is not only the relative cooling of the ocean water packages as they approach the polar regions that allows deep convection to occur, and in order to construct a complete diagnostic of the ocean density properties, ocean salinity must also be examined.

5.2.2 Salinity Response

The salinity response is slightly more diverse than the temperature signal. Due to the increase in temperature and the corresponding melting of land and sea ice, a lens of relatively fresh water forms in the surface layers of deep convection zones. Simultaneously, the layers directly beneath this, now prevented from mixing, become relatively salty. Combining these two effects acts to increase the gradient between surface and deep layers, generating a stronger physical barrier to mixing.

In the Labrador Sea downwelling region, the freshwater lens that forms is approximately 0.5 psu fresher than in the control state, and the layer immediately below this increases by 0.2 psu. The timing of salinity changes corresponds directly to the shallowing of the mixed layer, demonstrating that the relative salt changes are connected to the ability of the ocean to mix. As the convection shuts down, the deep ocean undergoes mild freshening; this is due to the response time of the deep ocean layers, which would re-equilibrate after approximately 1600 to 3000 years, possibly even longer in glacial climate states. The freshening occurs due to a decrease of the amount of salt that is transported into the deep ocean via downwelling. The surface layers below the freshwater bubble maintain their increased salinity, although this is restricted to the depth of the mixed layer, water below this retains the properties seen at the last possible mixing event. This effect is directly connected to the deeper ocean freshening, salt that can no longer be mixed down to the deep ocean due to density gradient changes is trapped in the upper layers of the ocean.

The GIN seas respond differently. A surface freshwater lens also forms here, although the salinification of the layer immediately below extending to the bottom of the mixed layer occurs much later in the simulation. Contrary to the response of the Labrador Sea, the deep ocean layers below the mixed layer undergo a progressive freshening. Here, the freshening has a greater magnitude due to the longer mixing time; surface freshening is able to be communicated to the deep ocean for an overall longer portion of the simulation before mixing in this downwelling zone shuts down. Once the mixing shuts down, the mild freshening of newly formed water packages in deep water formation is enhanced, since the portions of salt that would be mixed down no longer exist, increasing the freshwater anomaly in the deep ocean.

As with the temperature response, the signal seems to be amplified by a greater concentration of GHG, although the overall patterns stay similar. Including a dynamic ice sheet increases the freshening, which

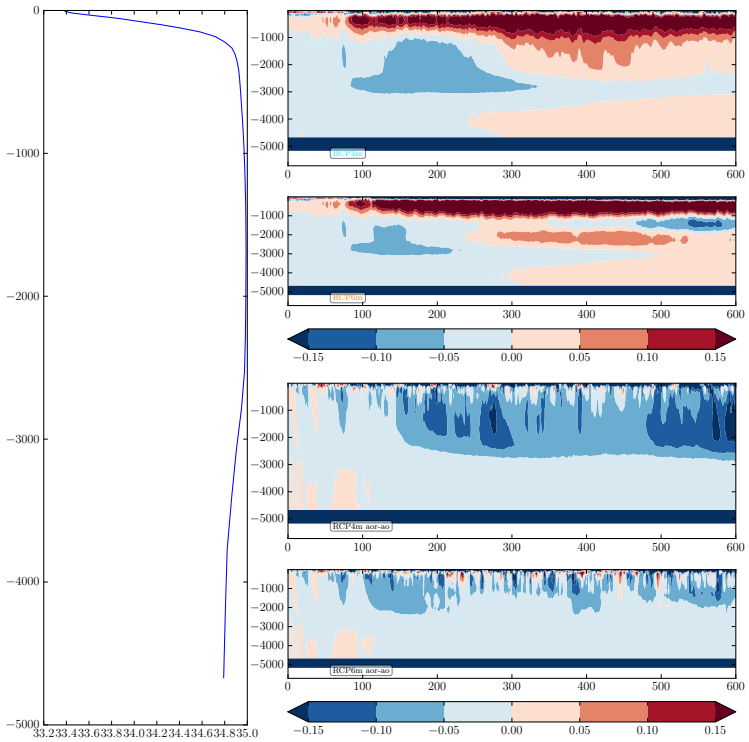

Figure 46: Response of Labrador Sea Salinity to 1% RCP Scenarios. A small freshwater lens forms in the uppermost layers, as can be seen in the upper two panels (`aoi-ctl`, RCP 4.5 in the first panel, RCP 6 in the second), followed immediately by a salty layer that forms due to limited convection. The entire water column is fresher in the simulation with dynamic ice sheets, as shown in the bottom two panels (`aoi-ao`)

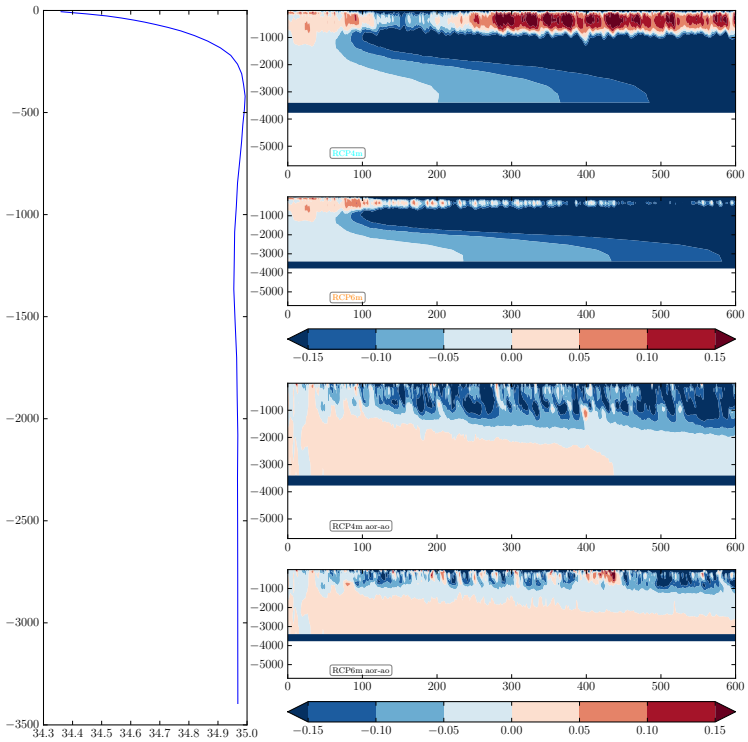

Figure 47: Greenland Sea Salinity Response. The freshwater lens is much more pronounced than in the LAB sea (shown in 43), and extends deep into the water column. This results in an increased density gradient, limiting convection and consequently shutting down circulation. The upper two panels show anomalies to the control state (`aoi-ctl`), whereas the lower to show differences introduced by the dynamic ice sheet component (`aoi-ao`)

will have the effect of further reducing the surface layer density, increases the amount of freshening in the upper ocean, modifying the buoyancy conditions, and consequently hampering convection.

6 CONCLUSIONS

6.1 IMPLICATIONS OF AMOC WEAKENING

As was mentioned in the introduction, the combination of surface and deep ocean circulation plays a vital role in the distribution of heat between the equatorial and polar latitudes. Due to a reduction in the ocean circulation from freshwater increase, a measurable decrease of heat transport can be seen. Observations place current heat transport in the Atlantic Ocean at 1.3 PW [11].

Decreases of heat transport can also be seen in the model simulations. Shown below are integrated heat transports over the entire Atlantic Basin for the control state, RCP4.5, and RCP6. The decreased northward transport is due to changes in the AMOC as well as associated slowing of the Gulf Current.

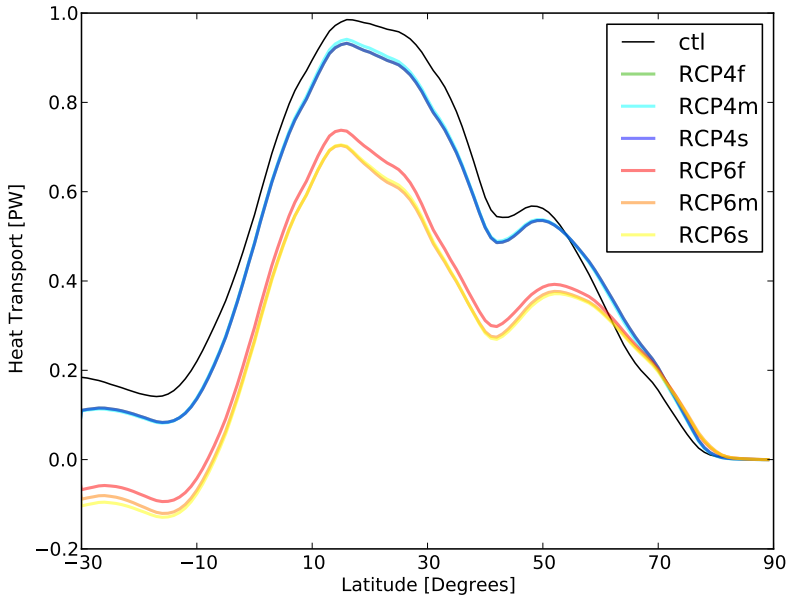

Figure 48: Northward heat transport in the Atlantic Ocean. A pronounced decrease in the amount of energy transported northwards is seen as a result of decreased meridional overturning circulation. Due to the very small differences of heat transported, several of the experiments are overlapping, RCP6 1% and RCP6 0.5% are nearly identical, as are all the RCP 4.5 experiments.

As can be seen, the control run generates a maximum heat transport of about 0.95 PW, whereas the RCP4.5 scenarios decrease this by 0.05 PW to 0.9 PW. In RCP6, the heat transport is reduced even further, and is only at 0.65 W by the end of the simulation period.

6.2 ANALOGIES TO PAST CLIMATE STATES

The behavior exhibited by the AMOC in this study has also been seen in paleoclimate studies. such as the work done by Srokosz et al. [45]. In fact, it has been suggested that past rapid climate changes, occurring on the order of several decades, can be linked to changes in the deep ocean circulation system. The AMOC itself seems to have more than one stable state, and while initially it was suggested that this was a simple "on/off" configuration, paleoevidence shows that there could be three distinct modes of operation. Rahmstorf characterizes these are "warm", "cold", and "off". [32]

The "warm" or interstadial mode, prevelant during interglacials corresponds best to what is seen in present day conditions, differing from the "cold" or stadial mode only in how deep into the ocean the North Atlantic water penetrates and in where it forms. Deep water formation occurs in the Nordic seas during interstadial mode, whereas it forms in the subpolar open ocean in stadial mode, corresponding to locations south of Iceland. The "off" mode does not feature any North Atlantic water, and consists solely of Antarctice Bottom Water. This is demonstrated in Figure 49, taken from Rahmstorf [32]

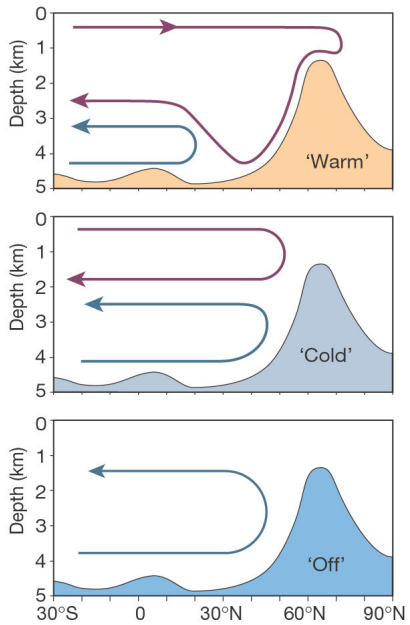

Figure 49: From Ramstorf 2002. Shown is a section along the Atlantic; the rise in bottom topography symbolizes the shallow sill between Greenland and Scotland. North Atlantic overturning is shown by the red line, Antarctic bottom water by the blue line.

Changes between these modes are theorized to be connected to large injections of freshwater, occurring through so-called Heinrich events. A massive discharge of icebergs calved from glaciers drift into the North Atlantic, where the eventual melting corresponds to a freshening of between 0.2 Sv to 0.4 Sv [9], although the actual strength of the injection events is still an area of active research. Other freshwater pulses may be introduced by ice dammed lakes in North America,

leading to pulses of a similar magnitude [28]. From such evidence, it is clear that the behavior of the AMOC is highly variables, and can change quite rapidly. The order of magnitude of freshwater introduced in these experiments (between 0.14 and 0.2 Sv, Fig 39) is similar to that seen in past climate states.

Freshwater may only be one mechanism of many that influence the behavior of the AMOC system. Studies by Knorr and Lohmann [16] suggest that changes in insulation and resulting sea ice dynamics could also cause AMOC shutdowns.

6.3 LIMITATIONS

As with any modeling study, there are several limitations that must be mentioned. First and foremost, it is important to understand that models are unable to predict or forecast the future of the climate system. Models can only simulate future climate possibilities based upon estimations of the evolution of various forcing factors, such as GHG levels. Therefore, the general goal of climate modeling studies is usually to gain a more detailed understanding about the processes operating within the climate system.

With this goal in mind, a few limitations should be noted. Firstly, the model resolution, being rather coarse, forces many small scale dynamic processes to be truncated. The inability of the ocean or the atmosphere to resolve motion on an eddy scale creates an unrealistic physical behavior in certain areas. Certain systems such as the Gulf Stream in the ocean, the downwelling processes in the Nordic Seas, or the Jet Stream in the atmosphere, being climate features that are comprised of such small scale eddies, are only represented in a limited fashion.

Secondly, it was not possible to introduce a form of tracer in the ocean, that would have allowed the distinction of freshwater changes due to ice sheet melting from other processes that impact ocean salinity. Incorporating such a numerical tracer would have allowed for a better understanding of the interaction of the ice sheet with other climate components.

A third major limitation was the technical development stage of the ice sheet model, RIMBAY. While the model has certainly improved since this first set of experiments was performed, at the time, the inability to simulate ice shelves, which would have had an impact on the fashion in which the Antarctic Ice Sheet responded to the climate; and more importantly for this study, the inability to allow the ice sheet edge, or grounding line, to migrate as the ice sheet grows and shrinks, severely impacts the numerical solution of ice sheet calving, which is the primary coupling to the ocean. Without calculating calving that occurs further in the "interior" of the ice sheet, being at the edge of an ice sheet that has retreated compared to the present day climate, a large amount of information is lost. Repeating the experiments with a new implementation of the ice sheet model would possibly yield much more realistic results. Precisely this improvement

is one of the more important next steps, more of which are presented below.

6.4 POSSIBLE NEXT STEPS AND OUTLOOK

Apart from the improvements to the RIMBAY ice sheet model already mentioned in the limitations, work has also been done on developing an ice sheet environment for the entire northern hemisphere rather than just including the Greenland Ice Sheet, allowing for a broader simulation.

Possible new applications of this model setup include simulation of past climate states to further validate the ice model, and to examine the response of the deep ocean circulation system in previous interglacial warm periods. The advantage of paleoclimate studies is the availability of corresponding geologic data, which would allow for intercomparsion projects between geochemical proxies and climate simulations.

If possible, it would be interesting to include the calved ice from the ice sheet model in the ocean as sea ice or, alternatively, to include a new iceberg subcompontent. This would allow for the simulation of dynamically responding climates with Heinrich events, further validating past paleoclimate analyses with numeric simulations. If such a model were forced with evolving CO_2 levels and orbital parameter variations and "naturally occurring" abrupt and rapid climate change would occur in the simulation, a major milestone of paleoclimate modeling would be achieved.

Already mentioned as a limitation in this study, some other groups, for instance work done at NCAR by Hu et al [10] or by Weijer [54] at the Los Alamos National Laboratory in New Mexico have suggested that including a highly resolved ocean component capable of simulating eddying currents increases the realism of the simulation, which would more closely corresponds to the system in the real world. The model used here was coarsely resolved by comparison. Repeating or adapting the experiments to a similar resolution might provide additional insight on how the system responds in the nordic seas on a eddy level. A higher resolution would also allow for the examination of climate modes, which have also been suggested to have a connection to the AMOC system. [19]

Finally, in order to determine bifurcation points within the AMOC system and to understand why certain scenarios allow for a recovery and others do not, it would be useful to preform several additional scenarios, varying not only the emission rate even further, but also including some additional IPCC scenarios. Decreasing the GHG level after a long integration time would answer questions about system recovery, showing if the ice sheet can recover from such a melting scenario or if the climate is forced into a different quasi-stable equilibrium. Increasing the integration time would allow the deep ocean to come further into equilibrium, allowing for examinations of the

temperature and salt features not only in the surface and intermediate layers but also in the deep layers.

6.5 SUMMARY

In conclusion, it has been shown that the North Atlantic basin and the ocean circulation systems within that basin are sensitive to freshwater input from a dynamic ice sheet model. Rather than using prescribed hosing, the climate system in this new `aoi` model configuration is able to dynamically simulate freshwater injections from an ice sheet. Using two kinds of model configuration, with fixed and with dynamic ice sheets, it could be determined that including ice sheets had a significant impact on both the atmospheric and oceanic response to various warming scenarios, and that the freshwater melt from the ice sheet has a dramatic effect on the density of the surface layers of the North Atlantic, impacting the formation rate of deep water, and consequently hampering the strength of the Atlantic Meridional Overturning Circulation. A decrease of this circulation has impacts on both regional and global transport, leading to a decrease in the amount of heat transported from the equatorial Atlantic to the sub polar latitudes, acting as a possible brake on atmospheric warming and additionally altering rainfall patterns and storm patterns in the North Atlantic. Other studies suggest that global signals are also seen, altering drought patterns in North America, Indian and Asian monsoon systems, shifts in the ITCZ, and changes in the global carbon cycle due to changes in marine biogeochemistry. Due to these impacts, the AMOC system is of crucial significance in regulating the global climate, and monitoring how the circulation responds to global warming will allow us to better understand how our planet is changing.

A GRAPHIC EXPLANATION, LEGENDS, AND ABBREVIATIONS

All graphics were produced using the `python` programming language. In case that there is any interest into how exactly this works, a sample script is available upon request.

The color scheme used in the legends of the figures presented in this work are always keyed as follows:

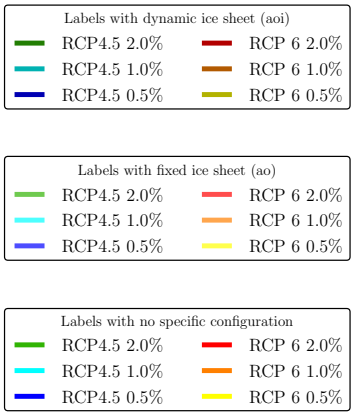

Figure 50: Legend for graphics

It should also be noted that the experiments are referred to by several different codes. `aor`, a code adopted from Dr. Wei Wei, the postdoc with whom I worked, stands for atmosphere-ocean-rimbay, the name of the ice sheet model. To clarify this, this has been replaced with `aoi` whenever possible, atmosphere-ocean-ice. Furthermore, the programming developed for running the coupled model required no special characters be used in the run names, therefore the 2%, 1%, and 0.5% runs are sometimes coded `f`, `m`, and `s`, for fast, medium, and slow emission rates.

When displaying results spatially, a similar pattern was often used. In a 4 panel setup, the upper two panels displayed absolute deviations from the control state for the scenario with lower GHG emissions, RCP4.5 on the left, and the deviations from the control state for the higher GHG scenario RCP6 on the right. These anomalies were of the form `aoi-ctl`, the value of the simulation with dynamic ice sheets less the value of the control state. The two panels directly below this are deviations between this shown state, `aoi`, and the state with fixed ice sheets, `ao`, being in the form `aoi-ao`.

Two dimensional time series were always shown in absolute values. Timeseries with depth, such as Figure 47 has the following setup. The large panel on the left side was a control profile with depth of a given variable, for instance salinity or temperature. Next to this, the 4 panels showed the progressing change to this profile for each year of the 600 year simulations, under certain conditions. The upper two panels showed the absolute change in the `aoi` setup, while the lower two panels showed the anomaly `aoi-ao`. This was chosen to demonstrate the effects of certain changes that occurred throughout the entire depth of the water column as time progressed.

B ADDITIONAL GRAPHICS

The graphics shown here represent the other emission scenarios at faster and slower rates than the ones shown in the main body. In general, similar patterns are seen, and the equilibrium state reached by the end of the experiments does not vary significantly from the RCP 4.5 and RCP6 1% runs shown earlier.

B.1 ATMOSPHERIC WARMING

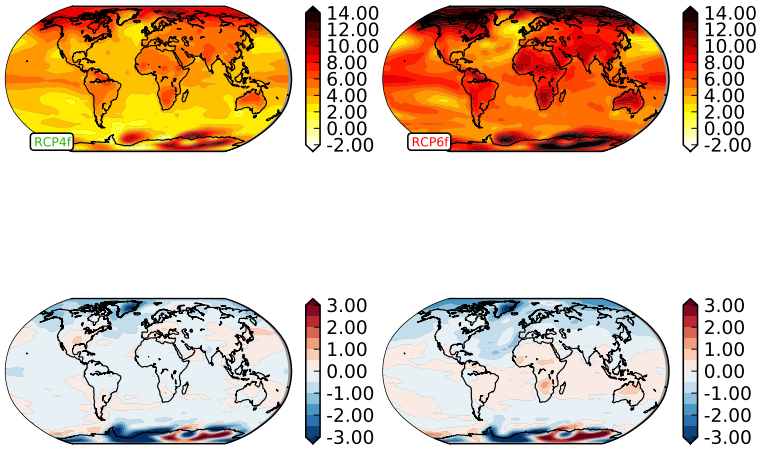

Figure 51: Atmospheric warming in 2% emission scenarios

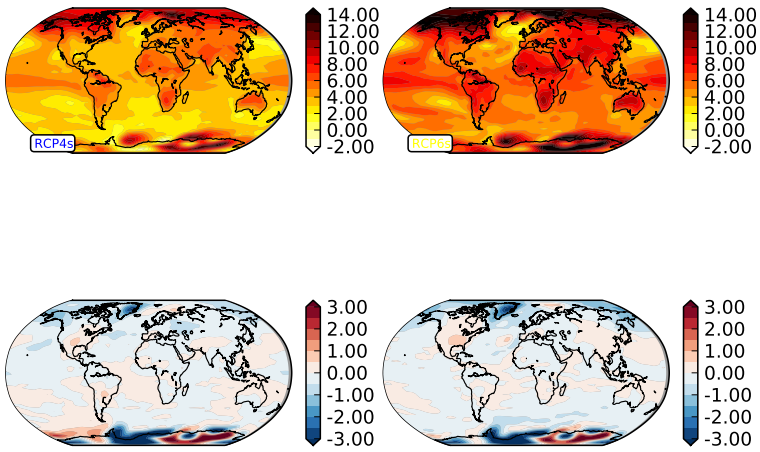

Figure 52: Atmospheric warming in 0.5% emission scenarios

B.2 SEA SURFACE TEMPERATURE

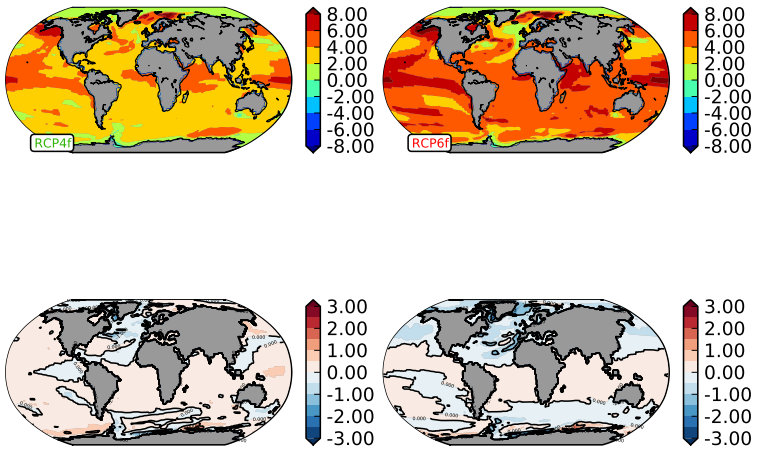

Figure 53: Sea surface temperature changes in the 2% emission rate scenarios.

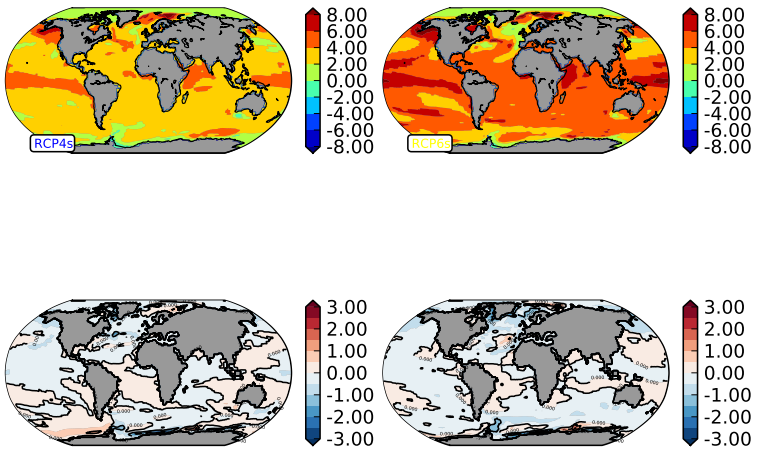

Figure 54: Sea surface temperature changes in the 0.5% emission rate scenarios.

B.3 SEA SURFACE SALINITY

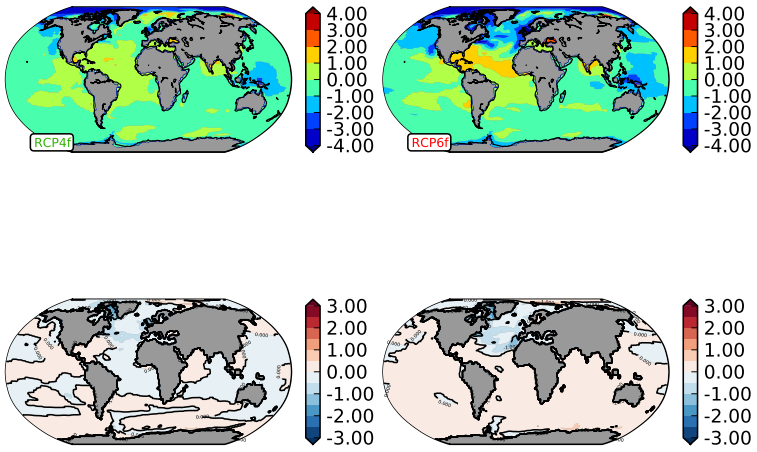

Figure 55: Sea surface salninity changes in the 2% emission rate scenarios.

B.4 ANTARCTICA

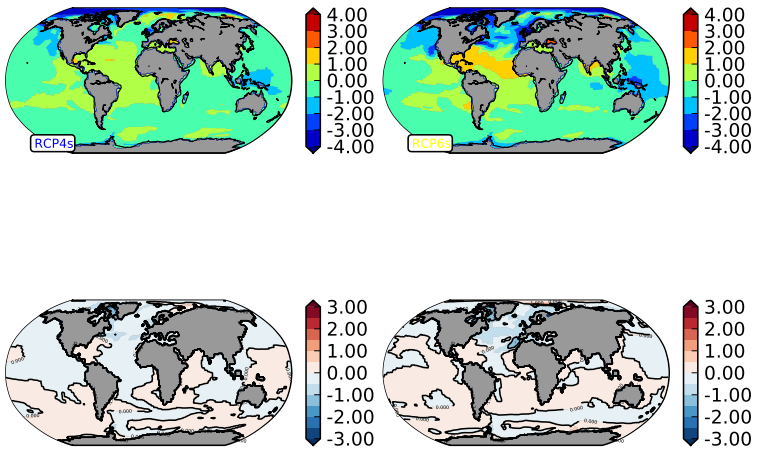

Figure 56: Sea surface salinity changes in the 0.5% emission rate scenarios.

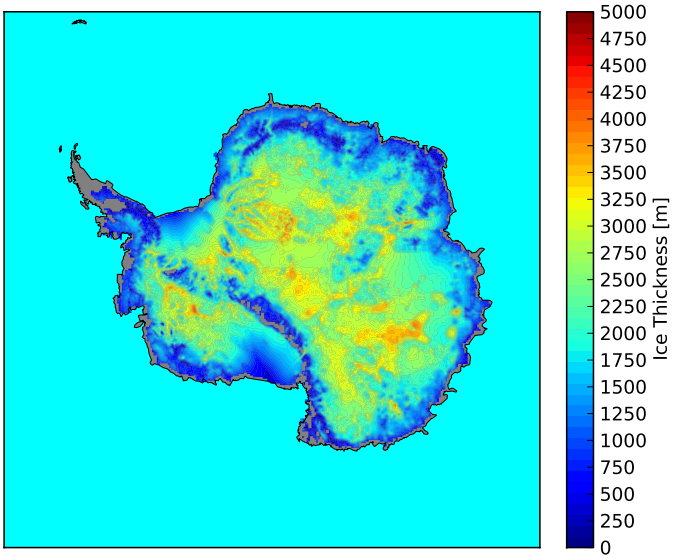

Figure 57: Simulated Antarctic Ice Sheet Thickness in RCP4.5 1%

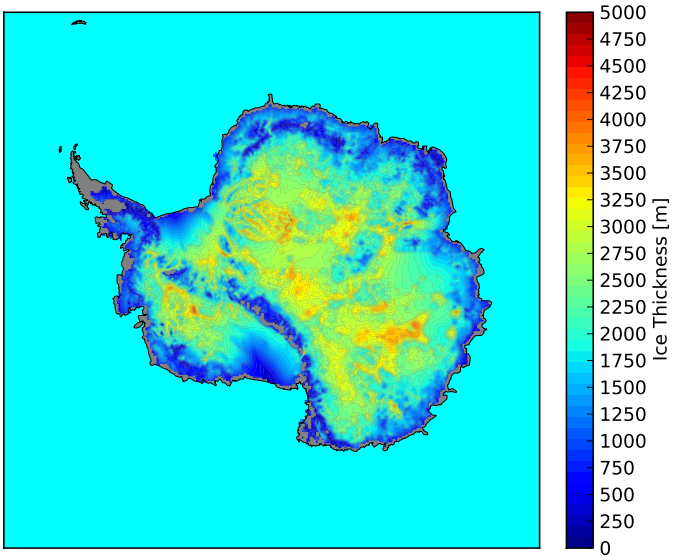

Figure 58: Simulated Antarctic Ice Sheet Thickness in RCP6 1%

BIBLIOGRAPHY

[1] J L Bamber, D J Baldwin, and S P Gogineni. A new bedrock and surface elevation dataset for modelling the Greenland ice sheet. *Annals of Glaciology*, 2003.

[2] D. Barbi, G Lohmann, and K Grosfeld. Ice sheet dynamics within an Earth system model: coupling and first results on ice stability and ocean circulation. *Geoscientific Model Development*, 2013.

[3] Anders A Bjork. An aerial view of 80 years of climate-related glacier fluctuations in southeast Greenland. *Nature Geoscience*, 5 (6):427, 2012.

[4] Jason E Box, David H Bromwich, Bruce A Veenhuis, Le-Sheng Bai, Julienne C Stroeve, Jeffrey C Rogers, Konrad Steffen, T Haran, and Sheng-Hung Wang. Greenland Ice Sheet Surface Mass Balance Variability (1988–2004) from Calibrated Polar MM5 Output*. *Journal of Climate*, 19(12):2783–2800, June 2006.

[5] Holger Braun, Marcus Christl, Stefan Rahmstorf, Andrey Ganopolski, Augusto Mangini, Claudia Kubatzki, Kurt Roth, and Bernd Kromer. Possible solar origin of the 1,470-year glacial climate cycle demonstrated in a coupled model. *Nature*, 438 (70695):208–211, November 2005.

[6] Anders E Carlson, Delia W Oppo, Rosemarie E Came, Allegra N LeGrande, Lloyd D Keigwin, and William B Curry. Subtropical Atlantic salinity variability and Atlantic meridional circulation during the last deglaciation. *Geology*, 36(12):991–994, December 2008.

[7] J L Chen. Satellite gravity measurements confirm accelerated melting of Greenland Ice Sheet. *Science*, 313:1958–1960, 2006.

[8] Jonathan M Gregory, Philippe Huybrechts, and Sarah C B Raper. Climatology: Threatened loss of the Greenland ice-sheet. *Nature*, 428(6983):616–616, April 2004.

[9] Sidney R Hemming. Heinrich events: Massive late Pleistocene detritus layers of the North Atlantic and their global climate imprint. *Reviews of Geophysics*, 42(1), 2004.

[10] A Hu, G A Meehl, W Han, and J Yin. Effect of the potential melting of the Greenland Ice Sheet on the Meridional Overturning Circulation and global climate in the future. *Deep Sea Research Part II: Topical Studies . . .* , 2011.

[11] W E Johns, M O Baringer, and L M Beal. Continuous, array-based estimates of Atlantic Ocean heat transport at 26.5 N. *Journal of . . .* , 2011.

[12] Nicola Jones. Arctic melt leads to weather extremes. *Nature Climate Change*, 2(4):221–221, April 2012.

[13] Manoj Joshi, Ed Hawkins, Rowan Sutton, Jason Lowe, and David Frame. Projections of when temperature change will exceed 2 [deg]C above pre-industrial levels. *Nature Climate Change*, 1(8): 407–412, October 2011.

[14] I Joughin, B E Smith, I M Howat, and T Scambos. Greenland flow variability from ice-sheet-wide velocity mapping. *Journal of Glaciology*, 56(197):415–430, 2010.

[15] G Knorr and G Lohmann. Southern Ocean origin for the resumption of Atlantic thermohaline circulation during deglaciation. *Nature*, 2003.

[16] G Knorr and G Lohmann. Rapid transitions in the Atlantic thermohaline circulation triggered by global warming and meltwater during the last deglaciation. *Geochemistry*, 2007.

[17] Gerhard Krinner and Gael Durand. Glaciology: Future of the Greenland ice sheet. *Nature Climate Change*, 2(6):396–397, 2012.

[18] T Kuhlbrodt, A Griesel, M Montoya, A Levermann, M Hofmann, and S. Rahmstorf. On the driving processes of the Atlantic meridional overturning circulation. *Reviews of Geophysics*, 45(2), April 2007.

[19] N Kvamstø and T Breiteig. The association between a weakening AMOC and the ENSO and NAO inter-annual variability. *AGU Fall Meeting Abstracts*, -1:0152, December 2010.

[20] Anne Le Brocq, Antony J Payne, and Andreas Vieli. An improved Antarctic dataset for high resolution numerical ice sheet models (ALBMAP v1). 2010.

[21] Timothy M Lenton, Hermann Held, Elmar Kriegler, Jim W Hall, Wolfgang Lucht, Stefan Rahmstorf, and Hans Joachim Schellnhuber. Tipping elements in the Earth's climate system. 2008.

[22] J. Marotzke. *Instabilities and multiple equilibria of the thermohaline circulation*. PhD thesis, Institut für Meereskunde Kiel, 1990.

[23] Toshihiko Masui, Kenichi Matsumoto, Yasuaki Hijioka, Tsuguki Kinoshita, Toru Nozawa, Sawako Ishiwatari, Etsushi Kato, P R Shukla, Yoshiki Yamagata, and Mikiko Kainuma. An emission pathway for stabilization at 6 Wm2 radiative forcing. *Climatic Change*, 109(1-2):59–76, August 2011.

[24] J F McManus, R Francois, J M Gherardi, L D Keigwin, and S Brown-Leger. Collapse and rapid resumption of Atlantic meridional circulation linked to deglacial climate changes. *Nature*, 428(6985):834–837, April 2004.

[25] M Meinshausen. How much warming are we committed to and how much can be avoided? *Climatic Change*, 2006.

[26] M Meinshausen, SJ Smith, K Calvin, and JS Daniel. The RCP greenhouse gas concentrations and their extensions from 1765 to 2300. *Climatic Change*, 2011.

[27] Richard H Moss, Jae A Edmonds, Kathy A Hibbard, Martin R Manning, Steven K Rose, Detlef P van Vuuren, Timothy R Carter, Seita Emori, Mikiko Kainuma, Tom Kram, Gerald A Meehl, John F B Mitchell, Nebojsa Nakicenovic, Keywan Riahi, Steven J Smith, Ronald J Stouffer, Allison M Thomson, John P Weyant, and Thomas J Wilbanks. The next generation of scenarios for climate change research and assessment. *Nature*, 463(7282):747–756, February 2010.

[28] Julian B Murton, Mark D Bateman, Scott R Dallimore, James T Teller, and Zhirong Yang. Identification of Younger Dryas outburst flood path from Lake Agassiz to the Arctic Ocean. *Nature*, 464(7289):740–743, April 2010.

[29] Glen P Peters, Gregg Marland, Corinne Le Quéré, Thomas Boden, Josep G Canadell, and Michael R Raupach. Rapid growth in CO2 emissions after the 2008–2009 global financial crisis. *Nature Climate Change*, 2(1):2–4, December 2011.

[30] S. Rahmstorf. Bif urcatii of the Atlantic thermohaline circulation in response to changes in the hydrological cycle. *Nature*, 1995.

[31] S. Rahmstorf. The thermohaline ocean circulation - a system with dangerous thresholds? *Climatic Change*, 46:247–256, 2000.

[32] Stefan Rahmstorf. Ocean circulation and climate during the past 120,000 years. *Nature*, 419(6903):207–214, September 2002.

[33] Stefan Rahmstorf, Michel Crucifix, Andrey Ganopolski, Hugues Goosse, Igor Kamenkovich, Reto Knutti, Gerrit Lohmann, Robert Marsh, Lawrence A Mysak, Zhaomin Wang, and Andrew J Weaver. Thermohaline circulation hysteresis: A model intercomparison. *Geophys. Res. Lett.*, 32(23):L23605, 2005.

[34] J Ridley, J M Gregory, P Huybrechts, and J Lowe. Thresholds for irreversible decline of the Greenland ice sheet. *Climate Dynamics*, 2010.

[35] J K Ridley, P Huybrechts, J M Gregory, and J A Lowe. Elimination of the Greenland Ice Sheet in a High CO 2Climate. *Journal of Climate*, 18(17):3409–3427, September 2005.

[36] E Rignot. Changes in the Velocity Structure of the Greenland Ice Sheet. *Science*, 311(5763):986–990, February 2006.

[37] E Rignot. Mass balance of the Greenland Ice Sheet from 1958 to 2007. *Geophys. Res. Lett.*, 35:L20502–, 2008.

[38] A Robinson. Multistability and critical thresholds of the Greenland ice sheet. *Nature Climate Change*, 2:429–432, 2012.

[39] E. Roeckner. *The atmospheric general circulation model ECHAM5, Part 1*, 2003.

[40] Joeri Rogelj, William Hare, Jason Lowe, Detlef P van Vuuren, Keywan Riahi, Ben Matthews, Tatsuya Hanaoka, Kejun Jiang, and Malte Meinshausen. Emission pathways consistent with a 2[thinsp][deg]C global temperature limit. *Nature Climate Change*, 1(8):413–418, October 2011.

[41] Oleg A Saenko, Andreas Schmittner, and Andrew J Weaver. The Atlantic–Pacific Seesaw. *Journal of Climate*, 2004.

[42] William J. Schmitz. *On the world ocean circulation. Volume I, Some global features/North Atlantic circulation*. Woods Hole Oceanographic Institution, Woods Hole, MA, 1996.

[43] N M Shapiro and M H Ritzwoller. Inferring surface heat flux distributions guided by a global seismic model: particular application to Antarctica. *Earth and Planetary Science Letters*, 2004.

[44] Donald Shepard. A two-dimensional interpolation function for irregularly-spaced data. In *Proceedings of the 1968 23rd ACM national conference*, pages 517–524, New York, New York, USA, 1968. ACM Press.

[45] M Srokosz, M Baringer, H Bryden, S Cunningham, T Delworth, S Lozier, J. Marotzke, and Rowan Sutton. Past, present, and future changes in the Atlantic meridional overturning circulation. *Bulletin of the American Meteorological Society*, 93(11):1663–1676, 2012.

[46] T F Stocker. CLIMATE CHANGE:The Seesaw Effect. *Science*, 282 (5386):61–62, October 1998.

[47] Thomas F Stocker and Andreas Schmittner. Influence of CO2 emission rates on the stability of the thermohaline circulation. *Nature*, 388(6645):862–865, August 1997.

[48] Allison M Thomson, Katherine V Calvin, Steven J Smith, G Page Kyle, April Volke, Pralit Patel, Sabrina Delgado-Arias, Ben Bond-Lamberty, Marshall A Wise, Leon E Clarke, and James A Edmonds. RCP4.5: a pathway for stabilization of radiative forcing by 2100. *Climatic Change*, 109(1-2):77–94, July 2011.

[49] T. Toniazzo, J M Gregory, and P Huybrechts. Climatic Impact of a Greenland Deglaciation and its Possible Irreversibility. *Journal of Climate*, 17:1–13, January 2004.

[50] R S W van de Wal, W Boot, M R van den Broeke, C J P P Smeets, C H Reijmer, J J A Donker, and J Oerlemans. Large and Rapid Melt-Induced Velocity Changes in the Ablation Zone of the Greenland Ice Sheet. *Science*, 321(5885):111–113, July 2008.

[51] M van den Broeke, J Bamber, J Ettema, E Rignot, E Schrama, W J van de Berg, E van Meijgaard, I Velicogna, and B Wouters. Partitioning Recent Greenland Mass Loss. *Science*, 326(5955):984–986, November 2009.

[52] I Velicogna. Acceleration of Greenland ice mass loss in spring 2004. *Nature*, 443:329–331, 2006.

[53] I Velicogna. Increasing rates of ice mass loss from the Greenland and Antarctic ice sheets revealed by GRACE. *Geophys. Res. Lett.*, 36(L19503), 2009.

[54] W. Weijer, M. E. Maltrud, M. W. Hecht, H. A. Dijkstra, and M A Kliphuis. Response of the Atlantic Ocean circulation to Greenland Ice Sheet melting in a stronglyeddying ocean model. *Geophysical Research Letters*, 39(9), 2012.

[55] P Wetzel, H. Haak, J Jungclaus, and E. Maier-Reimer. *The Max-Planck-Institute Global Ocean/Sea-Ice Model MPI-OM*, June 2007.

[56] Kirsten Zickfeld, Anders Levermann, M Granger Morgan, Till Kuhlbrodt, Stefan Rahmstorf, and David W Keith. Expert judgements on the response of the Atlantic meridional overturning circulation to climate change. *Climatic Change*, 82(3-4):235–265, March 2007.

COLOPHON

This document was typeset using the typographical look-and-feel `classicthesis` developed by André Miede. The style was inspired by Robert Bringhurst's seminal book on typography "*The Elements of Typographic Style*". `classicthesis` is available for both LaTeX and LyX:

http://code.google.com/p/classicthesis/

Final Version as of May 31, 2013 (`classicthesis` version 4.1).

ERKLÄRUNG

Ich versichere hiermit, dass ich die vorliegende Arbeit selbständig verfasse und keine anderen als die im Literaturverzeichnis angegebenen Quellen benutzt habe.

Alle Stellen, die wörtlich oder sinngemäß aus veröffentlichten oder noch nicht veröffentlichten Quellen entnommen sind, sind als solche kenntlich gemacht.

Die Zeichnungen oder Abbildungen in dieser Arbeit sind von mir selbst erstellt worden oder mit einem entsprechenden Quellennachweis versehen.

Diese Arbeit ist in gleicher oder ähnlicher Form noch bei keiner anderen Prüfungsbehörde eingereicht worden.

Frankfurt am Main, Juni 2013

Paul Gierz